ROTORDYNAMICS ANALYSIS FOR THE HPFTP (High Pressure Fuel Turbopump) OF THE SSME (Space Shuttle Main Engine)

FINAL REPORT

~~An Interim Progress Report for~~

NASA Contract NAS8-31233

SSME Turbopump Technology Improvements via Transient Rotordynamics Analysis

Submitted to

George C. Marshall Space Flight Center
National Aeronautics and Space Administration

by

The University of Louisville
Louisville, Kentucky 40208

Dr. Dara W. Childs
Professor of Mechanical Engineering
Principal Investigator

30 July 1980

INTRODUCTION

This report concerns the rotordynamics of the HPFTP (High Pressure Fuel Turbopump) of the SSME (Space Shuttle Main Engine), and is a sequel to several earlier studies of this unit by the author [1], [2], [3]. The results of both linear (stability and synchronous response) and transient nonlinear analyses are reported. The same analysis procedures are employed here as previously; however, the data defining the rotordynamic model differs in the following two regards:

(a) The most-recent MSFC case structural dynamics model is employed.

(b) New dynamic coefficients were developed in the course of this study for the HPFTP interstage seals [4], [5], and introduced into the rotordynamics model. A copy of reference [5] is enclosed as part of this final report.

The objective of the analysis reported herein was an examination of possible problems in moving from RPL to FPL conditions, and a review of prior analysis results with the updated rotordynamics model as described above. The following questions are examined by the analysis completed:

(a) What would be the influence on HPFTP rotordynamics of a change in interstage seals from the presently employed "smooth-stepped" design to a "smooth-straight" configuration?

(b) How sensitive are stability and synchronous results to changes in bearing stiffnesses and damping?

(c) What would be the influence on rotordynamic stability of a change from the present stiff symmetric bearing-carrier design to an asymmetric bearing-carrier configuration?

THE HPFTP ROTORDYNAMIC MODEL

The rotordynamic model used in this study basically resembles those employed by the author [1], [2], [3] and other rotordynamics investigators of the SSME turbopumps. The data and parameters which are required to define a rotordynamics model can be separated into those which are relatively well known and assumed fixed, and those which are known only within limits, and are to be varied.

Specified Data

In the present analysis, the following parameters are assumed to be known and fixed:

(a) rotor and case structural dynamic models,

(b) speed-dependent dynamic coefficients for seals,

(c) stiffness and damping coefficients for the balance piston,

(d) bearing carrier stiffnesses,

(e) bearing dead-band clearances, and

(f) imbalance magnitude and location.

In a recent study of the HPOTP (High Pressure Oxygen Turbopump), the bearing dead-band clearances could vary widely due to tolerance stackups. This is not the case with the HPFTP which operates with much smaller clearances on the order of 0.25×10^{-3} inches. A 6 gm-in imbalance magnitude, located between the turbine wheels, was used to represent the effect of irregular coating loss on the turbine blades. Appendix A provides the numbers used to define the balance of the data.

The sources for the data are as follows: The rotor structural dynamic model was developed by B. Rowan, Rocketdyne; while the case structural dynamic model was developed by MSFC. As noted earlier, the seal coefficients were developed by the author as documented in [4], [5]. The remaining data coincide with those currently employed by MSFC as provided by S. Winder in an annotated computer data listing.

Varied Data

The nominal radial stiffness model of the HPFTP bearings as a function of speed

was provided by S. Winder, and is based on A.B. Jones analysis results as modified due to experimental data. These bearing stiffnesses seem to be reasonable in that they yield the correct first-critical-speed location. However, the HPFTP bearings are the same as the HPOTP (High Pressure Oxygen Turbopump) preburner bearings, and estimates of the HPOTP bearings have varied markedly. Hence, in this study, the stiffness is varied by $\pm 25\%$ of nominal.

Bearing damping is modeled by a linear, constant, damping coefficient with the values C_s=0,20 lb sec/in.

A "customary" destabilizing mechanism acting on a rotor's turbines is the "Alford aerodynamic cross-coupling" force [6] which is modeled by

$$\begin{Bmatrix} F_x \\ F_y \end{Bmatrix} = \begin{bmatrix} 0 & k_T \\ -k_T & 0 \end{bmatrix} \begin{Bmatrix} X \\ Y \end{Bmatrix} \; ; \quad k_T = \frac{\beta T}{D_p H}$$

where T is the turbine torque, D_p is the average pitch diameter of the turbine blades, H is the average height, and β is the "change of thermodyanmic efficiency per unit of rotor displacement, expressed as a fraction of blade height." The physical rationale for these forces is based on an increase in blade efficiency with decreasing tip clearance. The parameter β is varied here from unity to three.

No attempt is made to model impeller-diffuser forces similar to those calculated by J. Colding-Jorgensen [7] for a plain volute configuration, and more recently for the vaned-diffuser of the HPOTP. No such calculations have been made for the HPFTP impellers. Since these forces are assumed to be proportional to density, they will clearly be smaller for the HPFTP than the HPOTP.

Based on earlier results with the HPOTP [8], the influence of drive and load torques is not included in the present study.

LINEAR STABILITY AND SYNCHRONOUS RESPONSE RESULTS

Introduction

This section provides results based on linear synchronous response and stability calculations employing the procedures outlined in reference [2]. The results presented should be interpreted in light of the known nonlinear effects of bearing clearances [9]. Specifically, bearing clearances have a softening effect in lowering the apparent critical speed location, and cause a reduction in the peak magnitude of rotor response at the nonlinear* critical speed, as opposed to the zero-clearance linear critical speed. However, at running speeds below the nonlinear critical speed, amplitudes are increased with increasing bearing clearances. Note further in examining the linear results of this section that the axial balance-piston coupling between the rotor and case is not included. However, this is included in the transient model, whose results are included in the next section.

Figure 1 illustrates the reference coordinate system. The Z axis of this figure is seen to be aligned with the nominal axis of rotation for the HPFTP. As explained in [2], stability and synchronous response calculations are based on coupled rotor-case modes, which are calculated from separate case data (excluding the HPFTP rotor), free-free rotor modal data, and linear bearing stiffnesses. Separate modes are calculated for both the X-Z and Y-Z planes.

Orthotropic Bearing Carrier Design

Previous rotordynamics analysis of the HPFTP suggest that stability could be markedly improved by using an orthotropic bearing carrier with orthogonal stiffnesses of 1.75×10^5 and 5.0×10^5 lbs/in respectively. This configuration requires bearing damping, and employs the original grooved interstage seal design. Listed below are the orthotropic support and damping cases examined, together with their onset speed of instability results.

---

*Peak-amplitude running speed.

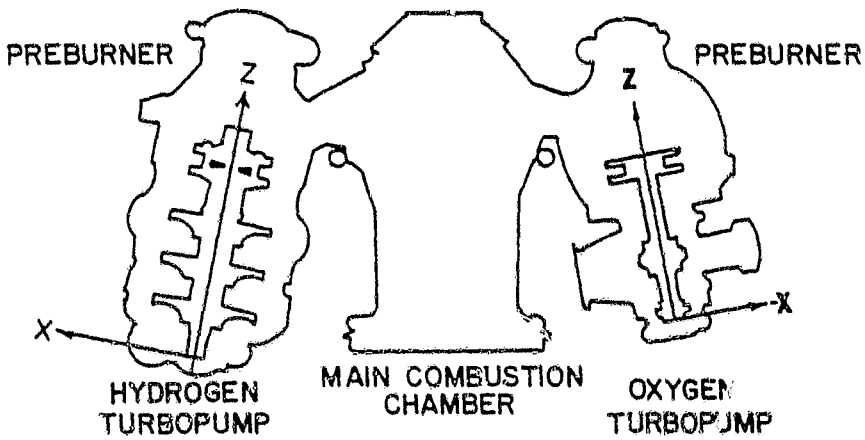

Figure 1. Local coordinate system for HPFTP analysis

(a) K_{sx}=1.75 X 10^5 lb/in, K_{sy}=5.0 X 10^5 lb/in

C_s=5 lb sec/in: ω_s=26,110 rpm

C_s=20 lb sec/in: ω_s=49,710 rpm

(b) K_{sx}=5.0 X 10^5 lb/in, K_{sy}=1.75 X 10^5 lb/in

C_s=5 lb sec/in: ω_s=26,140 rpm

C_s=20 lb sec/in: ω_s=49,170 rpm

The damping support constant C_s corresponds to a linear "dash-pot" in parallel with the support stiffness.

These stability results are not as attractive as previous predictions for orthotropic bearing supports. Specifically, in prior analyses support orthotropy caused the rotor to be stable relatively independent of support damping. With the present relatively-soft structural dynamic model, rotordynamic stability is primarily achieved by increased damping, and not by orthotropy. Note that stability results are relatively indifferent to the alignment of the bearing orthotropy axes with either the X-Z or Y-Z planes.

Figures 2 and 3 illustrate synchronous response results for C_s=20 lb sec/in. Bearing reactions are seen to be quite low for either alignment of the bearing orthotropy axes. In these figures, and throughout this report, bearing numbers 1 through 4 refer, respectively, to the pump outboard, pump inboard, turbine inboard, and turbine outboard bearings.

Conventional, Symmetric, Bearing-Carrier Design

Table 1 summarizes stability results for stepped and straight interstage seal designs for a 25% variation in nominal bearing stiffness with the two support damping coefficients, C_s=5,20 lb sec/in. The entry ζ(FPL) denotes the percent of critical damping at FPL, with ω_s continuing to denote the onset speed of instability.

The results presented are insensitive to changes in support damping. Except for the soft 0.75 K_b / stepped-seal combination, the onset speed of instability results are largely insensitive to changes in bearing stiffness or interstage seal

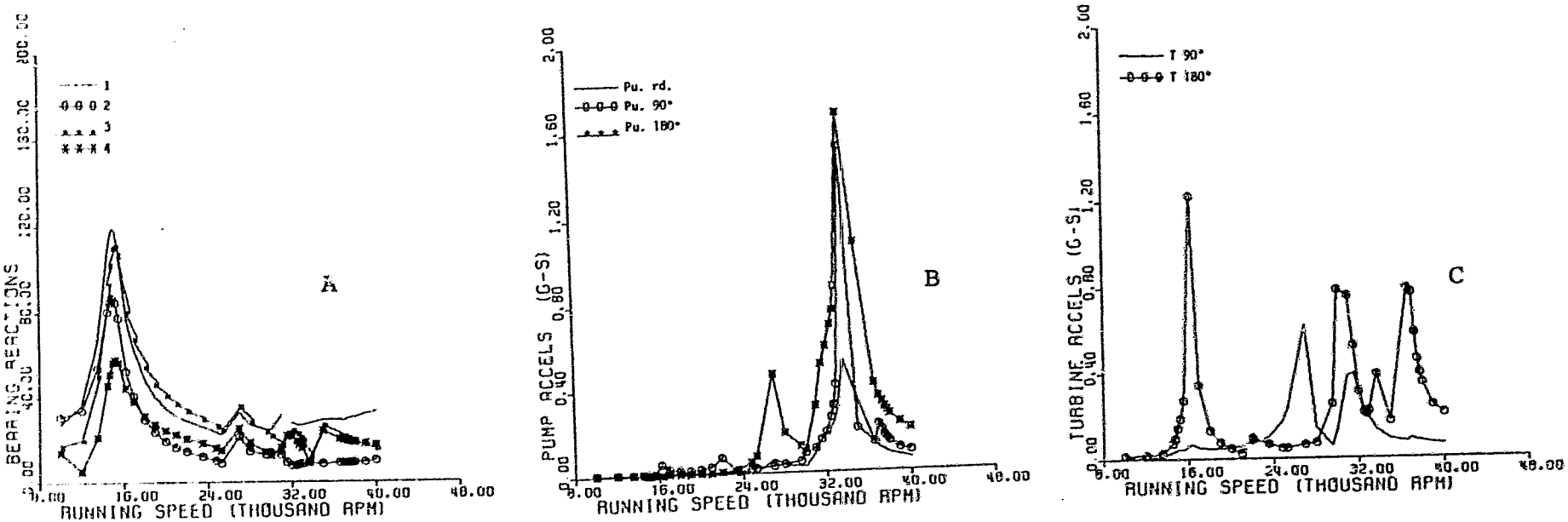

Figure 2 : Synchronous response results for orthotropic bearing carriers (K_{sx}=1.75 X 10^5 lb/in, K_{sy}=5.0 X 10^5 lb/in) for C_s=20 lb sec/in.

(a) bearing reactions (lbs)
(b) pump accel. levels (g's)
(c) turbine accel. levels (g's)

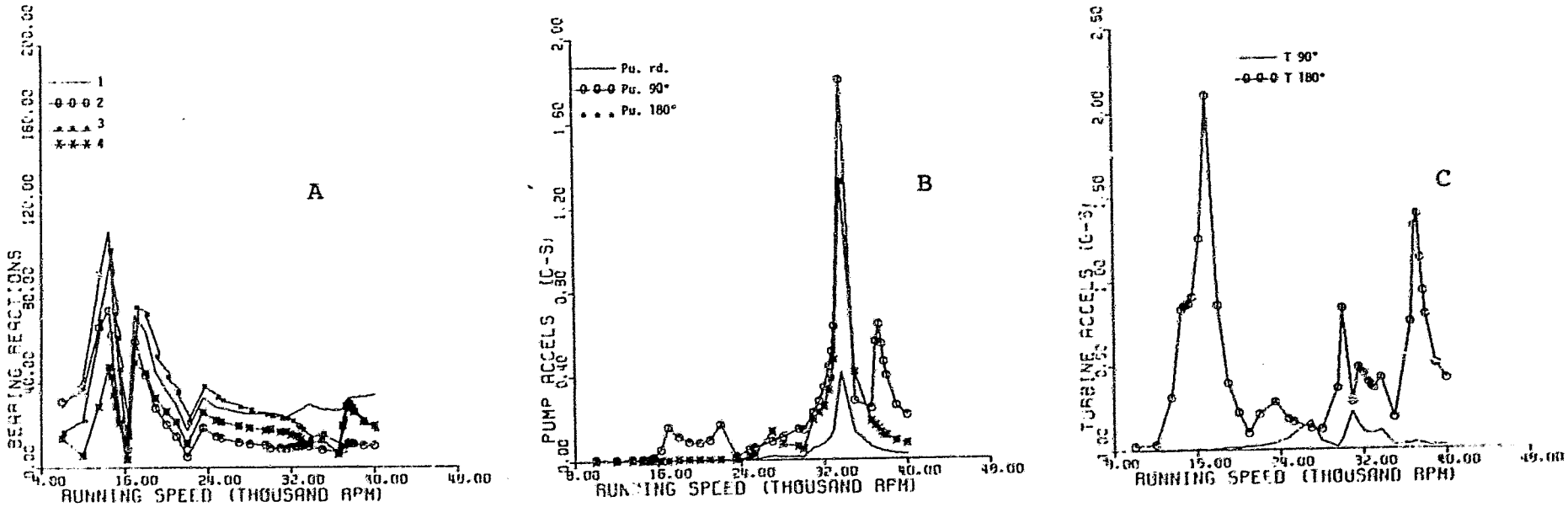

Figure 3 : Synchronous response results for orthotropic bearing carriers (K_{sx}=5.0 X 10^5 lb/in, K_{sy}=1.75 X 10^5 lb/in) for C_s=20 lb sec/in.

(a) bearing reactions (lbs)
(b) pump accel. levels (g's)
(c) turbine accel. levels (g's)

Stepped Seal

0.75 K_b	C_s=5	ω_s=74,544	ζ(FPL)=1.15%
	C_s=20	ω_s=75,000	ζ(FPL)=1.16%
1.0 K_b	C_s=5	ω_s=54,733	ζ(FPL)=0.88%
	C_s=20	ω_s=54,900	ζ(FPL)=0.89%
1.25 K_b	C_s=5	ω_s=53,663	ζ(FPL)=2.9%
	C_s=20	ω_s=54,597	ζ(FPL)=2.5%

Straight Seal

0.75 K_b	C_s=5	ω_s=51,634	ζ(FPL)=1.5%
	C_s=20	ω_s=51,890	ζ(FPL)=1.5%
1.0 K_b	C_s=5	ω_s=52,605	ζ(FPL)=1.5%
	C_s=20	ω_s=52,833	ζ(FPL)=1.6%
1.25 K_b	C=5	ω_s=53,782	ζ(FPL)=1.6%
	C=20	ω_s=53,930	ζ(FPL)=1.6%

Table 1. Onset speed of instability results for the symmetric bearing carrier with stepped and straight seals for 25% variation in bearing stiffnesses.

designs. The interstage seal design becomes slightly more stable with reduced bearing stiffness, while the converse situation holds for the straight seal design.

Figure 4 illustrates the reduction in onset speed of instability for the stepped and interstage seal designs due to an increase in the Alford cross-coupling term. These results are for the nominal bearing stiffness coefficients C_s=5 lb sec/in. Note that the straight-seal design is better able to withstand increases in β than the stepped seal, although either design has a comfortable speed margin for stability.

Figures 5 through 7 illustrate synchronous imbalance results for the stepped interstage seal design for 0.75 K_b, 1.0 K_b, and 1.25 K_b bearing stiffness definitions. These results are for 6 gm-in imbalance between the turbine wheels, and correspond to support damping of C_s=5 lb sec/in. The peak bearing loads are predicted for a critical speed in the vicinity of 32,000 rpm, and are moderately reduced for the stiff bearing (1.25 K_b) design. The pump inboard bearing is predicted to experience the largest load on the order of 2000 lbs. However, the associated turbine accel. levels are predicted to be between 20 and 60 g's, which is markedly higher than measured results for the HPFTP.

Figures 8 through 10 provide the same results for the straight-seal configuration as figures 5 through 7 provide for the stepped-seal. The bearing reactions loads are markedly reduced by the change in seals; however, the accel. levels are not proportionately reduced, and continue to be predicted at much higher levels than those which have been measured. The straight interstage seal configuration is seen to be quite insensitive to bearing stiffness variations.

In examining the results of figures 5 through 10, recall that the bearing clearance effect is not included. The bearing dead-band will markedly reduce the peak bearing loads. The following conclusions may be reached from an examination of these figures:

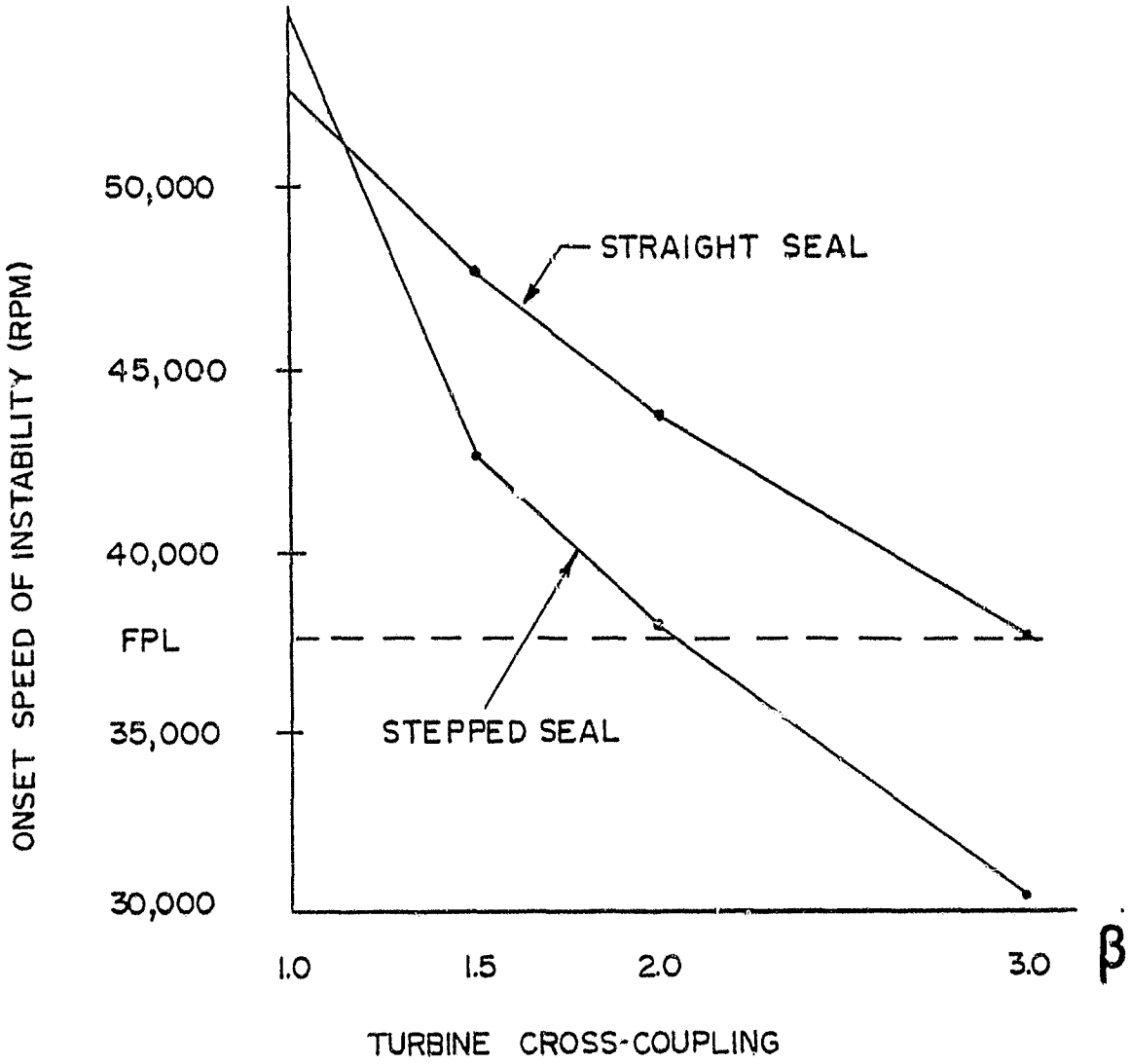

Figure 4 : Onset speed of instability results versus Alford cross-coupling coefficient β for straight and stepped interstage seal designs.

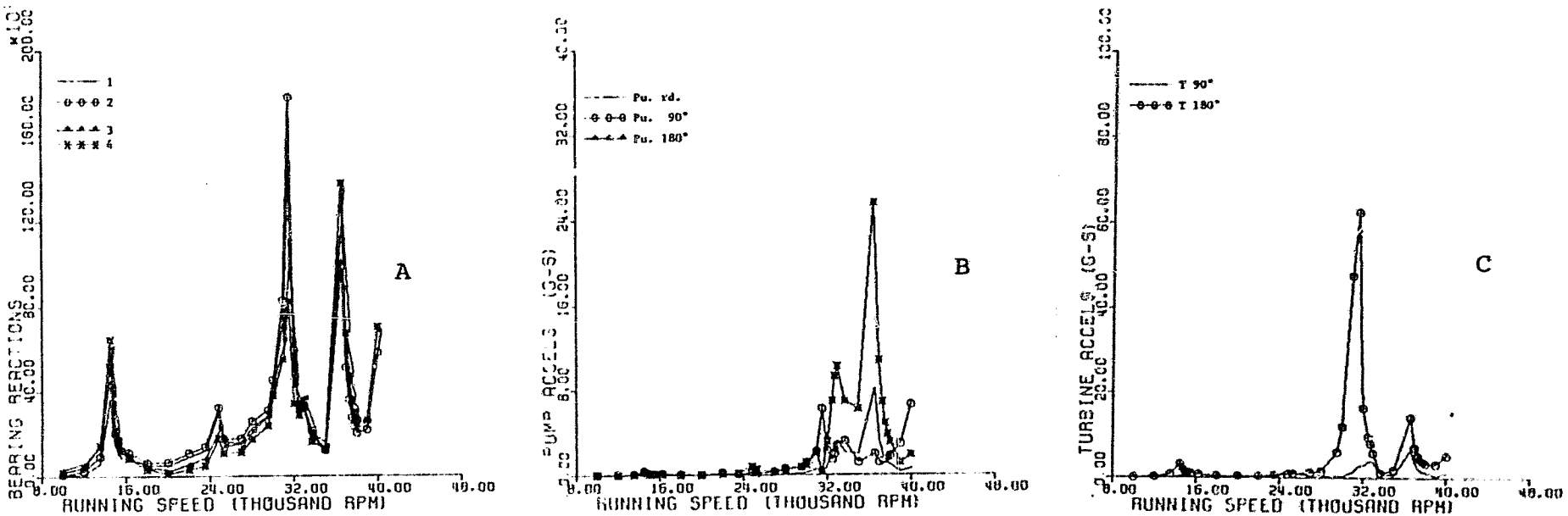

Figure 5 : Stepped-seal synchronous response results for $0.75K_b$ bearing stiffnesses, C_s=5 lb sec/in; 6 gm-in imbalance between turbine wheels

(a) bearing reactions (lbs)
(b) pump accel. levels (g's)
(c) turbine accel. levels (g's)

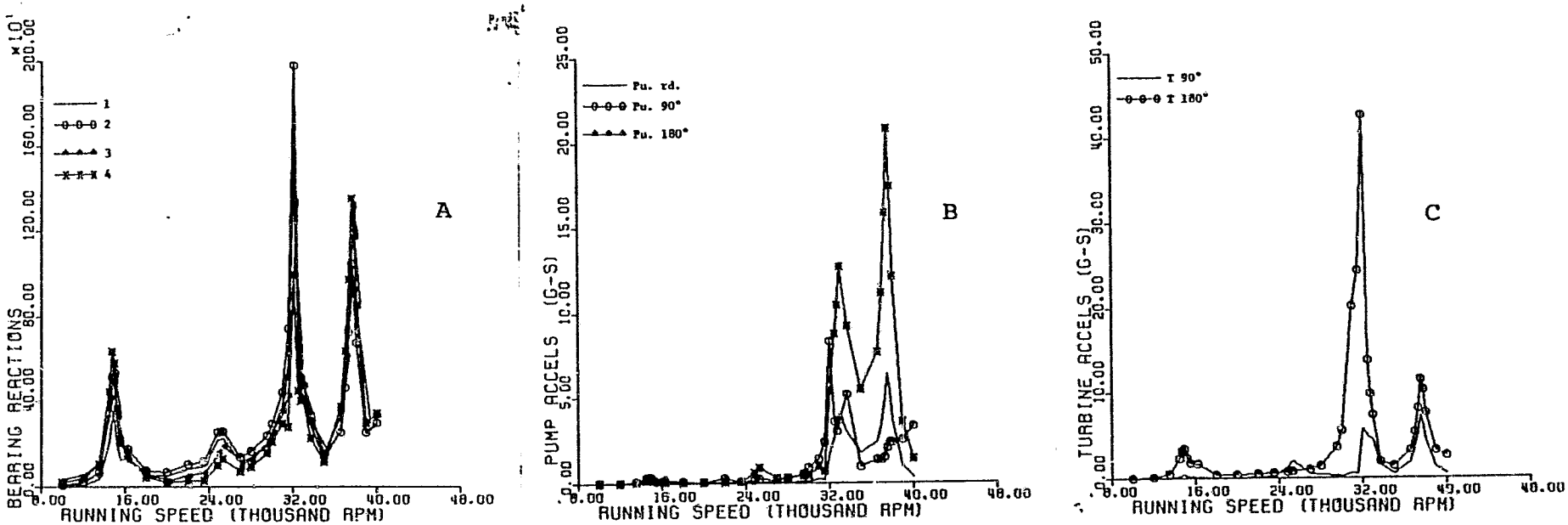

Figure 6 : Stepped interstage-seal synchronous imbalance response results for 1.0 K_b nominal bearing stiffnesses; C_s=5 lb sec/in; 6gm-in imbalance between turbine wheels.

(a) bearing reactions (lbs)
(b) pump accel. levels (g's)
(c) turbine accel. levels (g's)

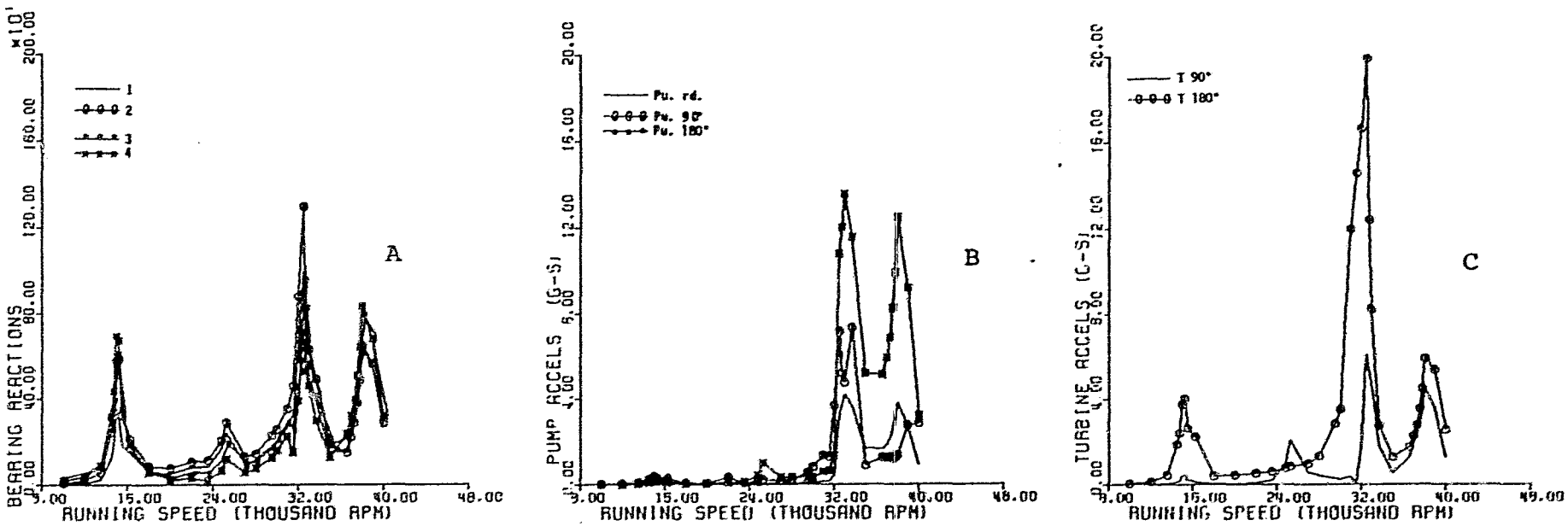

Figure 7 : Stepped interstage-seal synchronous imbalance response results for 1.25 K_b nominal bearing stiffnesses, C_s=5 lb sec/in; 6 gm-in imbalance between turbine wheels.

(a) bearing reactions (lbs)
(b) pump accel. levels (g's)
(c) turbine accel. levels (g's)

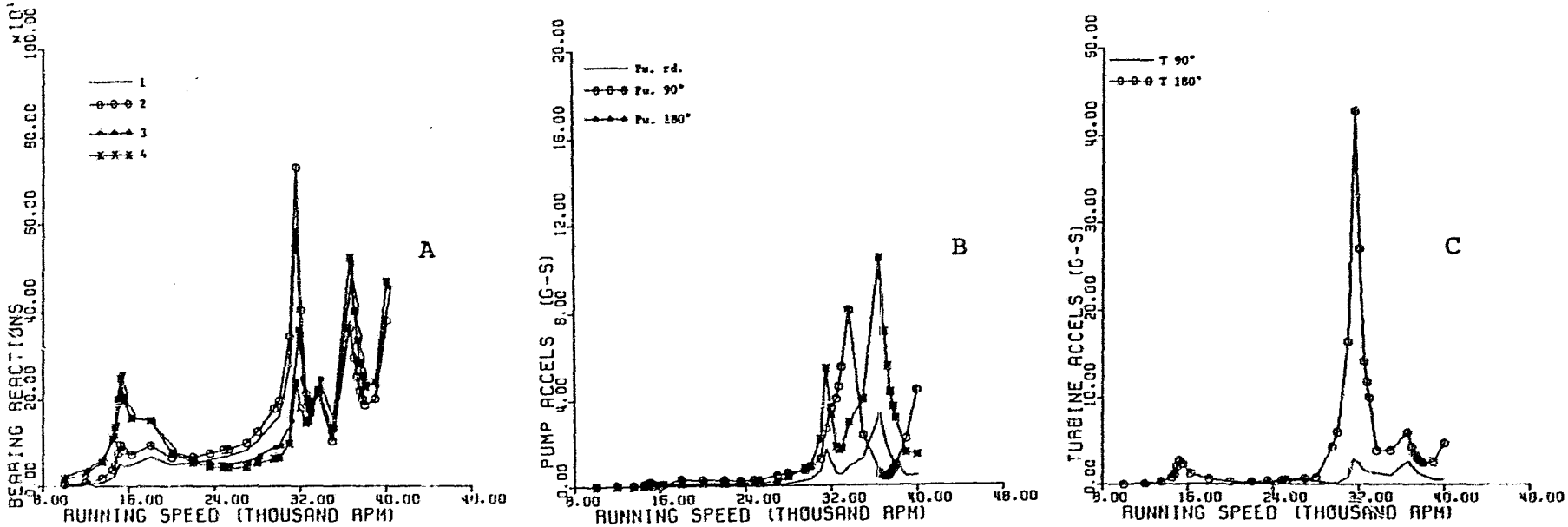

Figure 8 : Straight interstage-seal synchronous imbalance response results for 0.75 K_b nominal bearing stiffnesses; C_s=5 lb sec/in; 6 gm-in imbalance between turbine wheels.

(a) bearing reactions (lbs)
(b) pump accel. levels (g's)
(c) turbine accel. levels (g's)

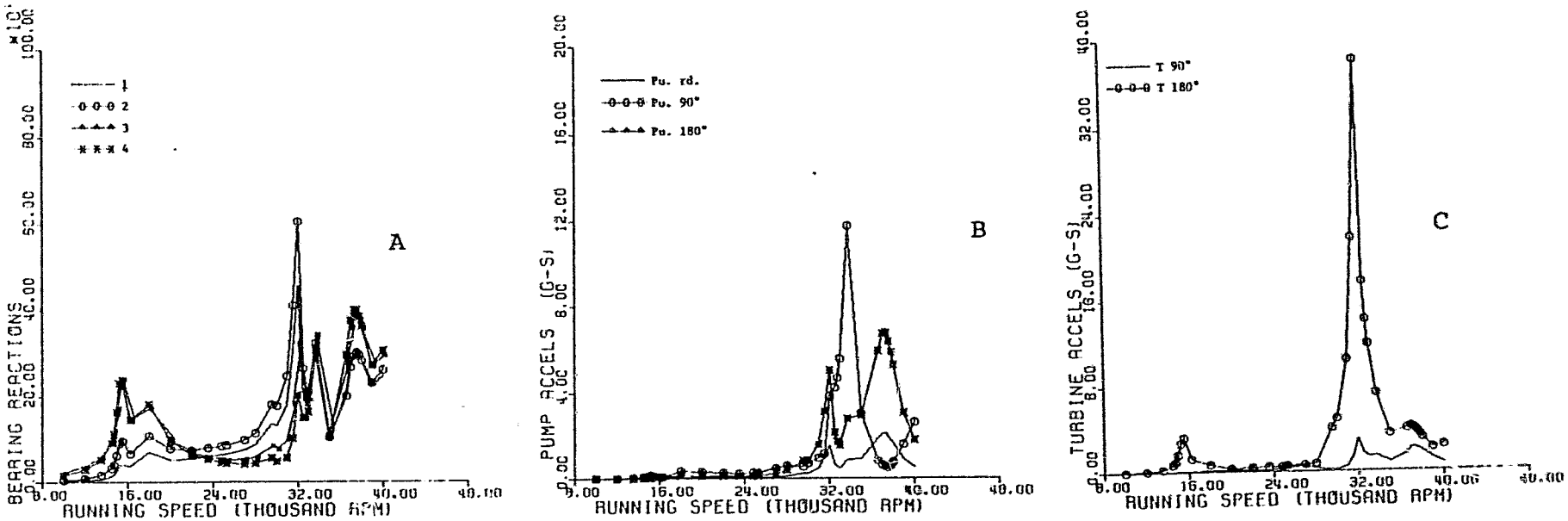

Figure 9 : Straight interstage-seal synchronous imbalance response results for 1.0 K_b nominal bearing stiffness; C_s=5 lb sec/in; 6 gm-in imbalance between turbine wheels.

(a) bearing reactions (lbs)
(b) pump accel. levels (g's)
(c) turbine accel. levels (g's)

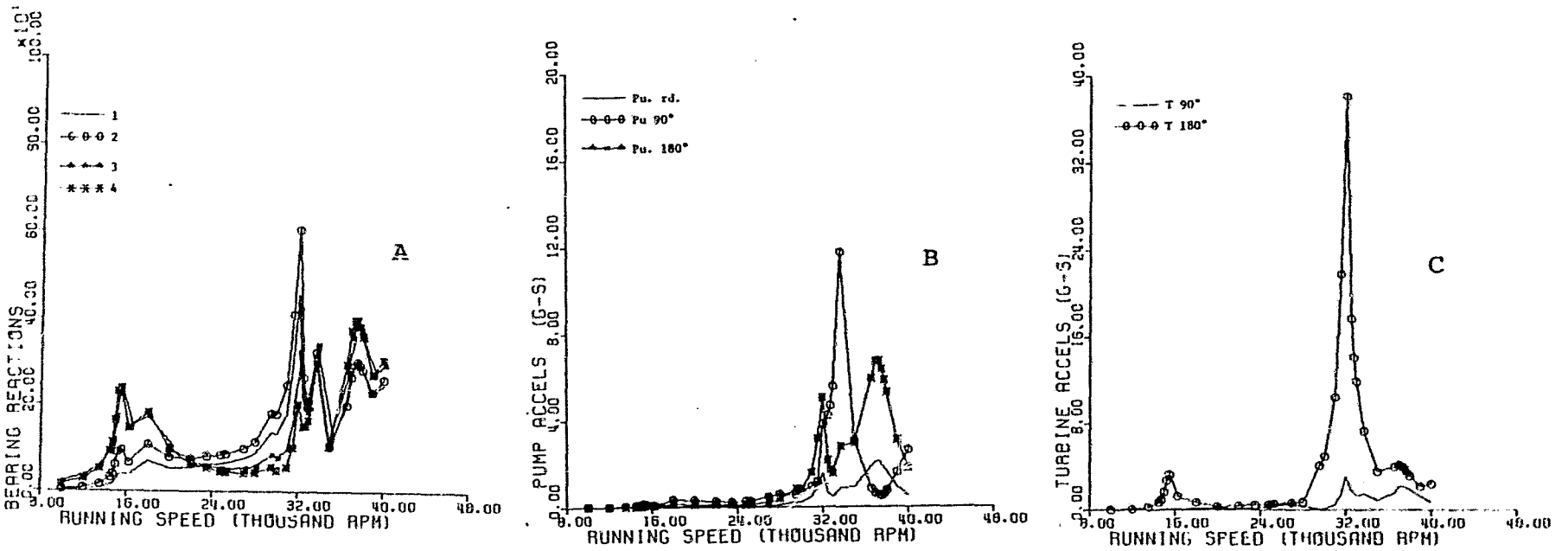

Figure 10 : Straight interstage-seal synchronous imbalance response results for 1.25 K_b nominal bearing stiffness; C_s=5 lb sec/in; 6 gm-in imbalance between turbine wheels.

(a) bearing reactions (lbs)
(b) pump accel. levels (g's)
(c) turbine accel. levels (g's)

(a) The straight interstage seal configuration is preferrable to the stepped, because it yields markedly smaller bearing loads.

(b) With the current case structural dynamics model, peak bearing loads are predicted at speeds around 32,000 rpm, which is below RPL. Hence, the linear synchronous response results actually predict smaller loads at FPL than RPL and lower speeds.

TRANSIENT NONLINEAR ANALYSIS RESULTS

As noted in the introduction section, the principal concern in this study is potential problems to be encountered in moving from RPL to FPL operating conditions. The analysis results reported in the preceding section address this concern via linear analysis procedures, while the results presented here consider the same question using transient nonlinear analysis techniques. The essential physical nonlinearity in the turbopump is the bearing "dead-band" clearance on the order of 0.25×10^{-3} inches.

Simulations were conducted for the nominal 1.0 K_b bearing stiffnesses, zero bearing damping, and straight and stepped-seal configurations. The results of a uniform deceleration from steady-state initial conditions at FPL to RPL for the stepped and straight configurations are illustrated in figures 11 and 12, respectively. The stepped-seal configuration shows a sharp peak in the vicinity of 35,800 rpm with high associated bearing loads on the order of 2000 to 2400 lbs; however, the associated pump and turbine accel. levels are not excessive, approaching 12 g's on the pump 90 accel. output. The results presented in figure 12 for the straight-seal-coefficient simulation are much more encouraging. The critical in this case occurs at approximately 37,200 rpm, with peak bearing loads on the order of 600 rpm.

Peak bearing loads for the stepped seal configuration were calculated for a steady running speed of 35,808 rpm with the following results:

R_1 = 2000 lbs $\qquad$ R_3 = 2300 lbs

R_2 = 2200 lbs $\qquad$ R_4 = 2400 lbs

The associated pump and turbine accel. levels for this steady-state operating conditions are:

G(Pump rad.) = 3 g's $\qquad$ G(Turbine 90°) = 1.0 g's

G(Pump 90°) =10 g's $\qquad$ G(Turbine 180°)= 2.0 g's

G(Pump 180°) =10 g's

Peak bearing loads for the straight-seal configuration were calculated at FPL conditions with the following results:

R_1 = 400 lbs $\qquad$ R_3 = 500 lbs

R_2 = 400 lbs $\qquad$ R_4 = 500 lbs

The associated pump and turbine accel. levels are:

G(Pump rad.) = 2.0 g's $\qquad$ G(Turbine 90°) = 1.2 g's

G(Pump 90°) = 7.0 g's $\qquad$ G(Turbine 180°)= 1.5 g's

G(Pump 180°) = 6.0 g's

The unmistakeable conclusion to be reached from these results is that predicted bearing loads are markedly reduced for the straight seal as opposed to the stepped-seal coefficients. The basic question which remains to be answered; however, is "How good are the calculated seal coefficients?" To the extent that they are an accurate measure of the seal's relative dynamic properties, the straight seal is obviously to be preferred.

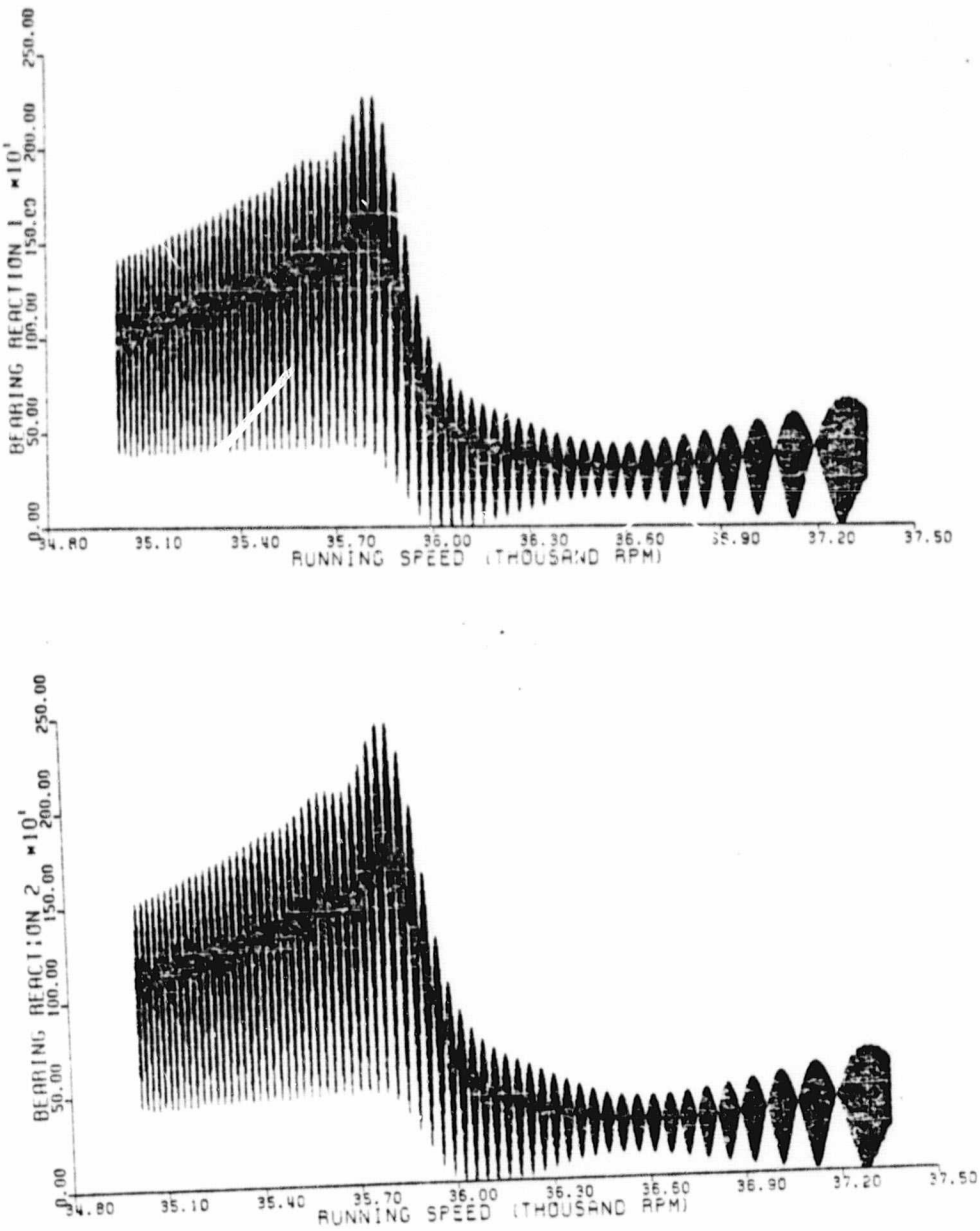

Figure 11 : Simulation of deceleration from FPL to RPL for the stepped-seal configuration.

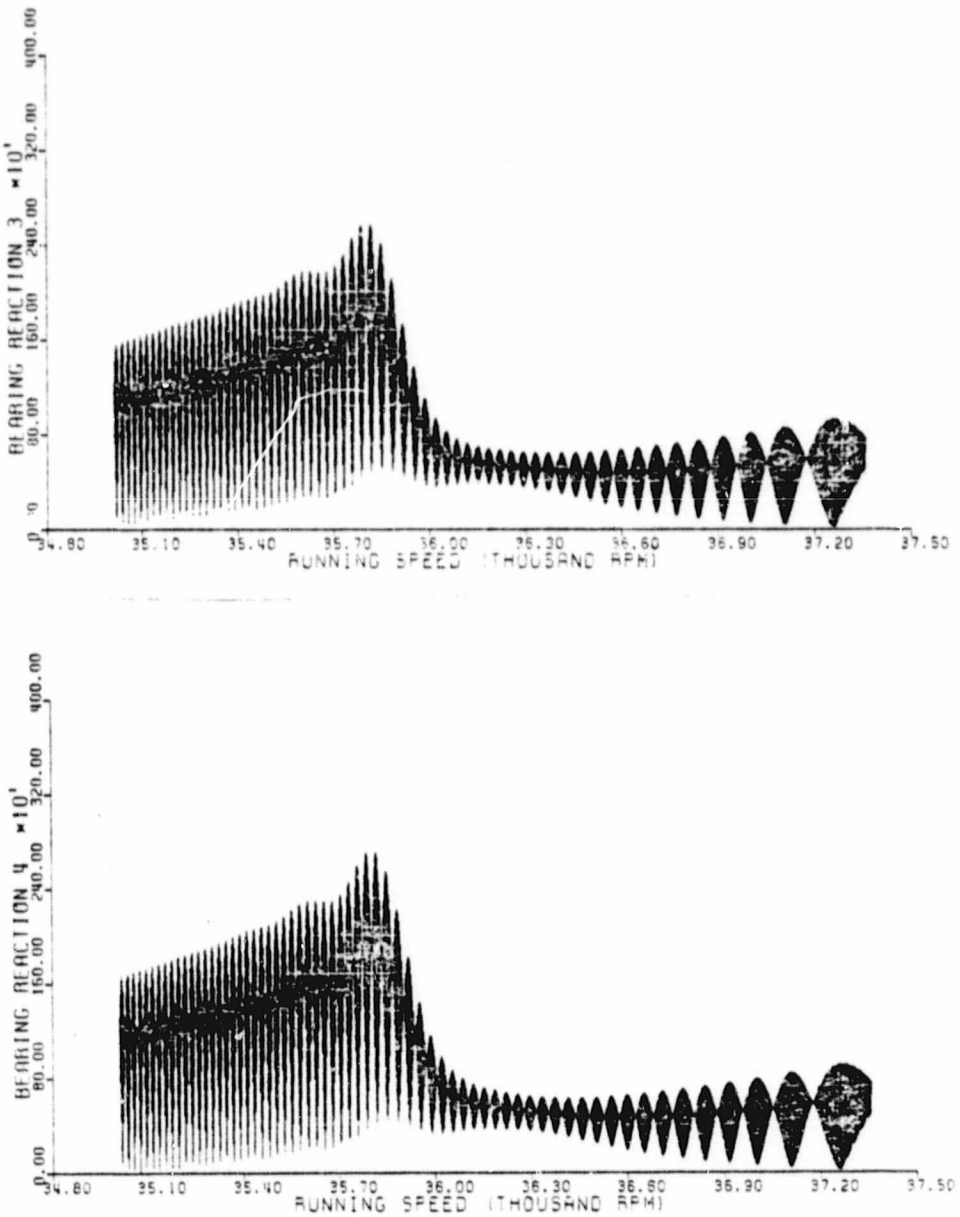

Figure 11 : Simulation of deceleration from FPL to RPL for the stepped-seal configuration.

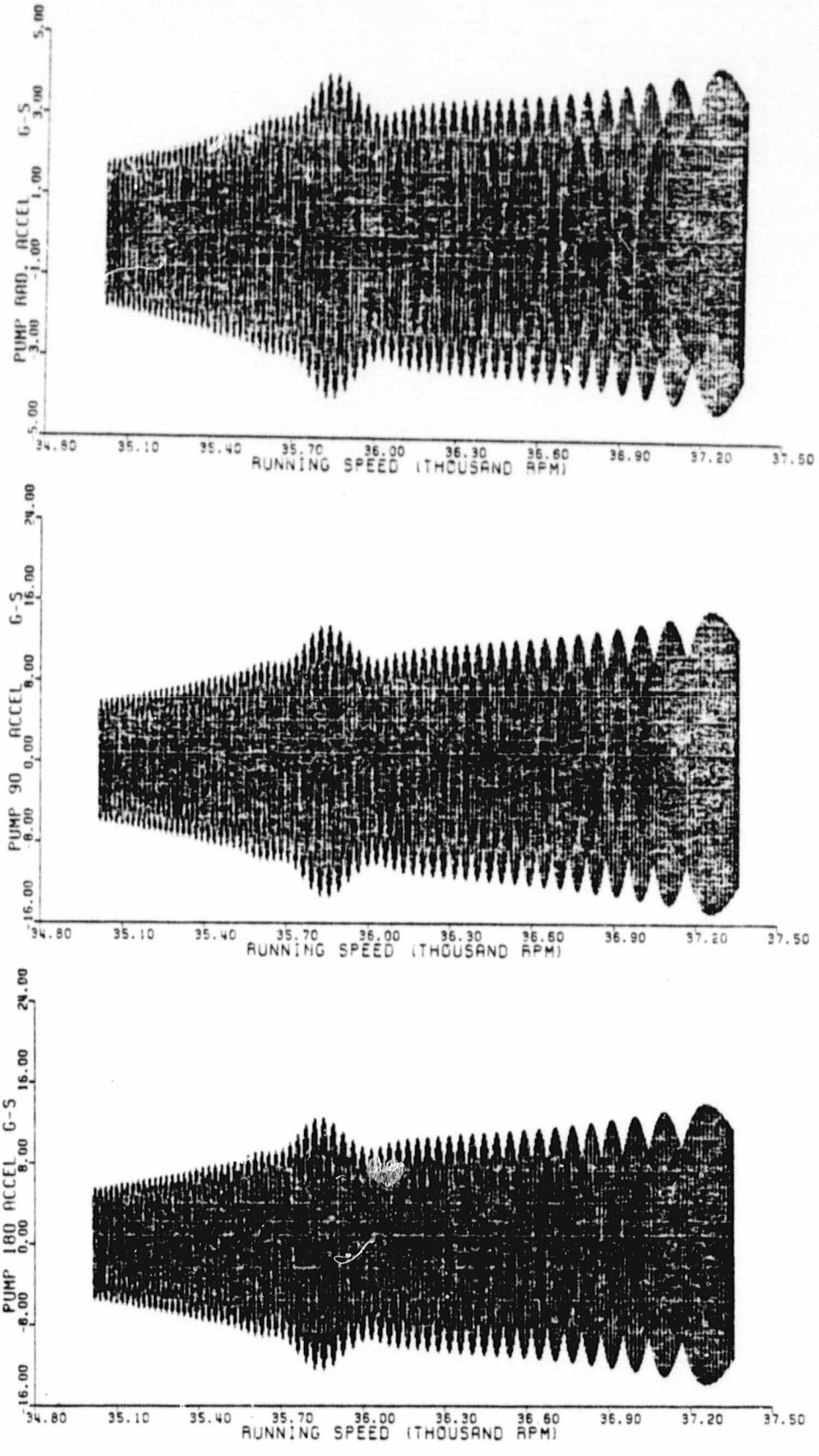

Figure 11 : Simulation of deceleration from FPL to MPL for the stepped-seal configuration.

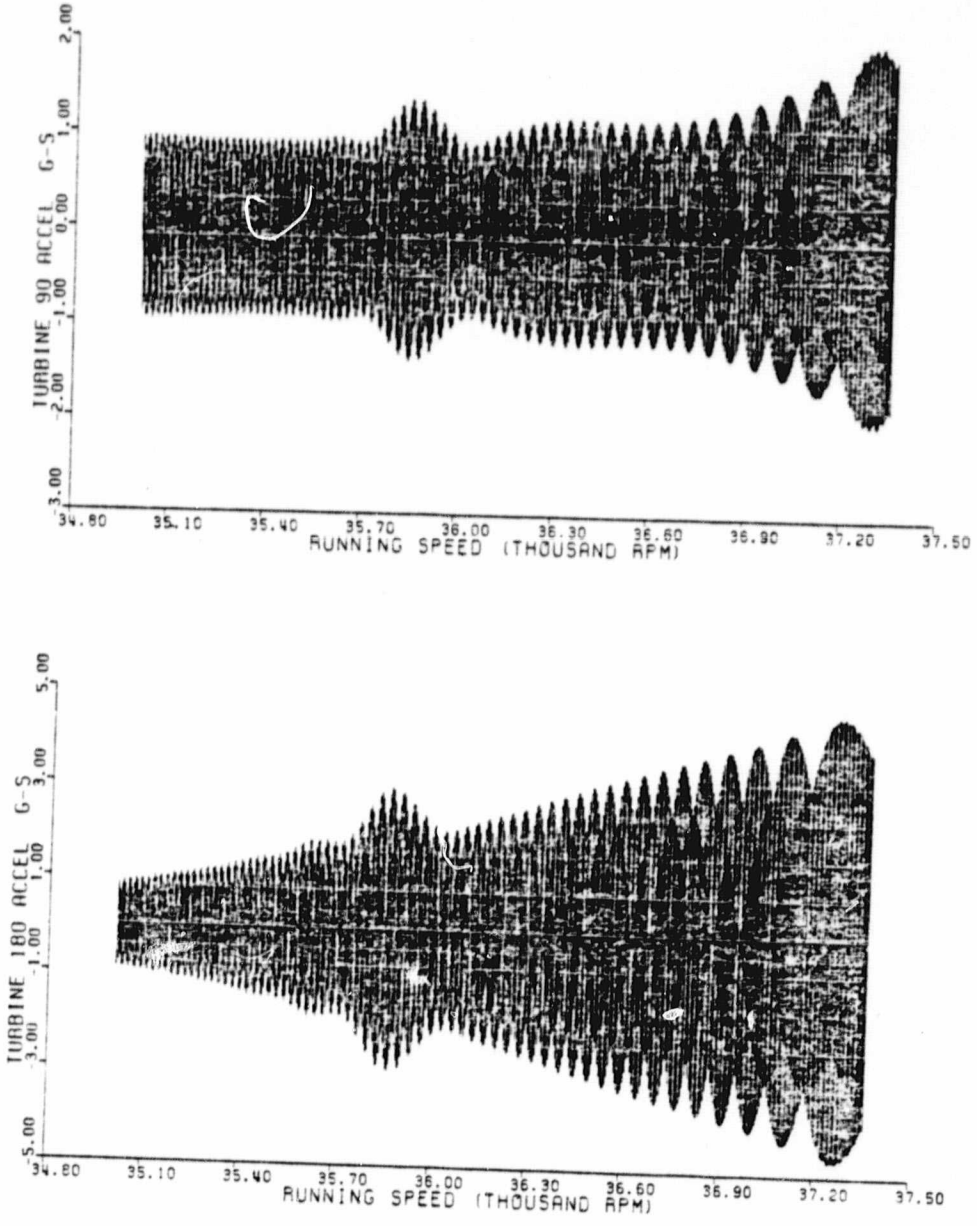

Figure 11 : Simulation of deceleration from FPL to RPL for the stepped-seal configuration.

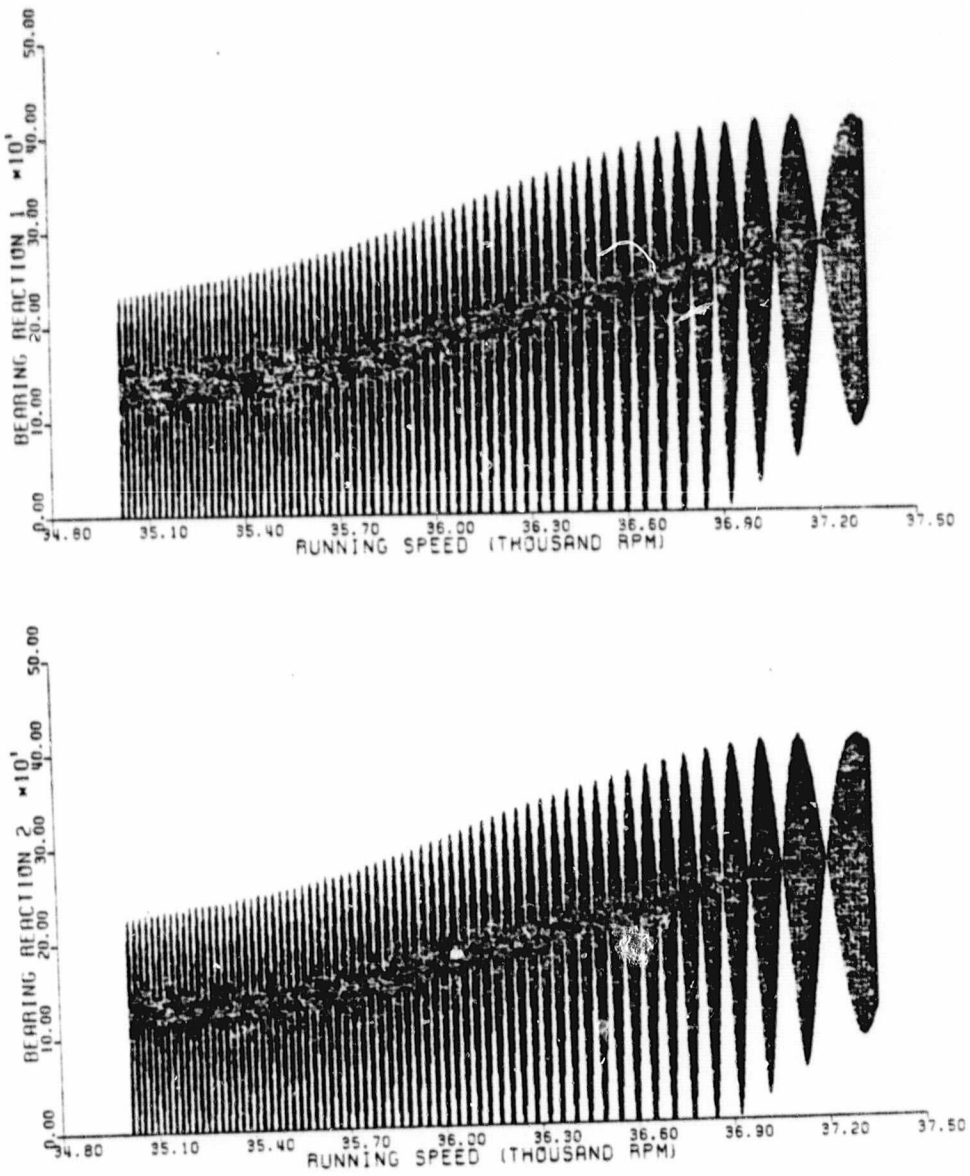

Figure 12 : Simulation of deceleration from FPL to RPL for the straight-seal configuration.

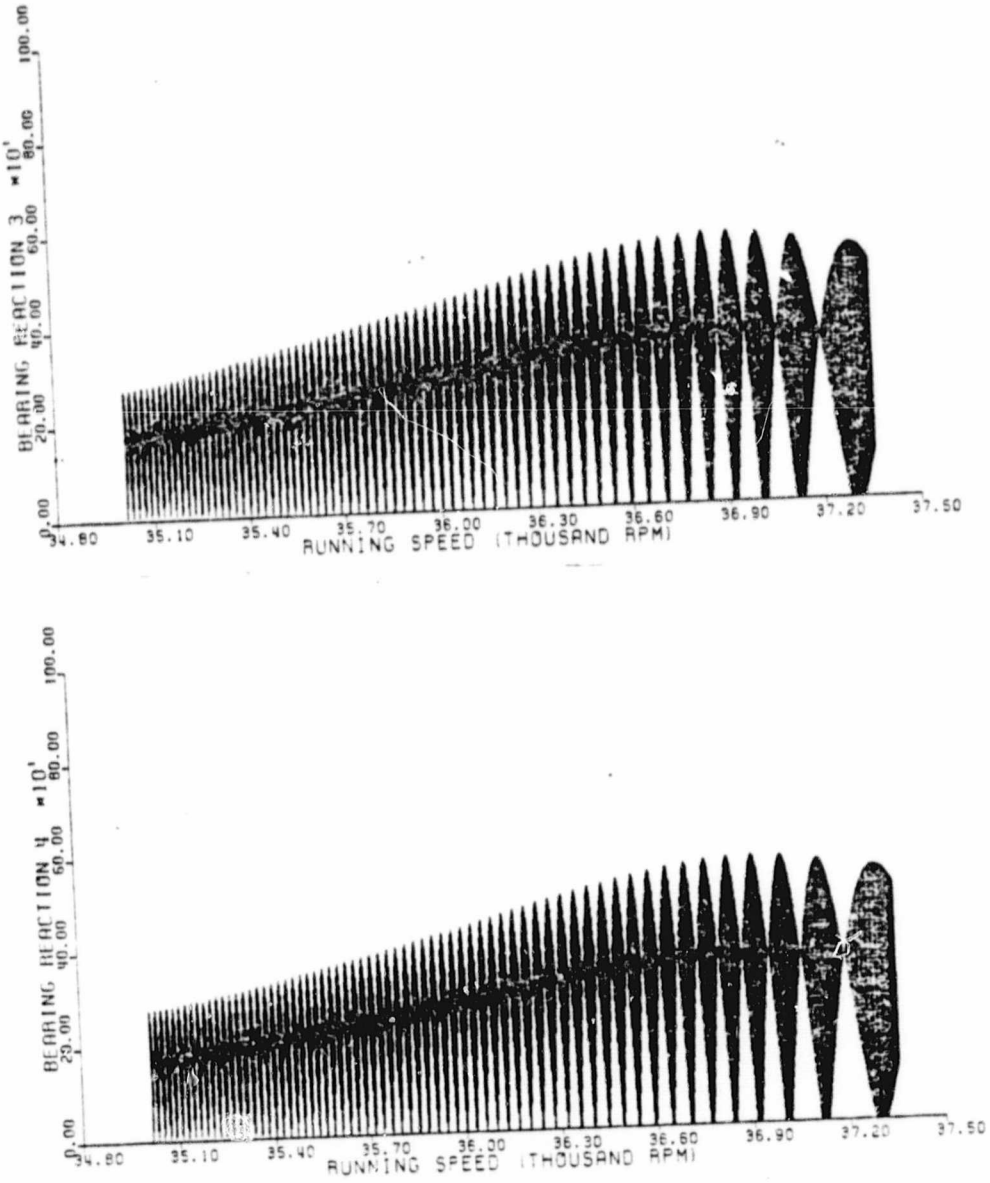

Figure 12 : Simulation of deceleration from FPL to RPL for the straight-seal configuration.

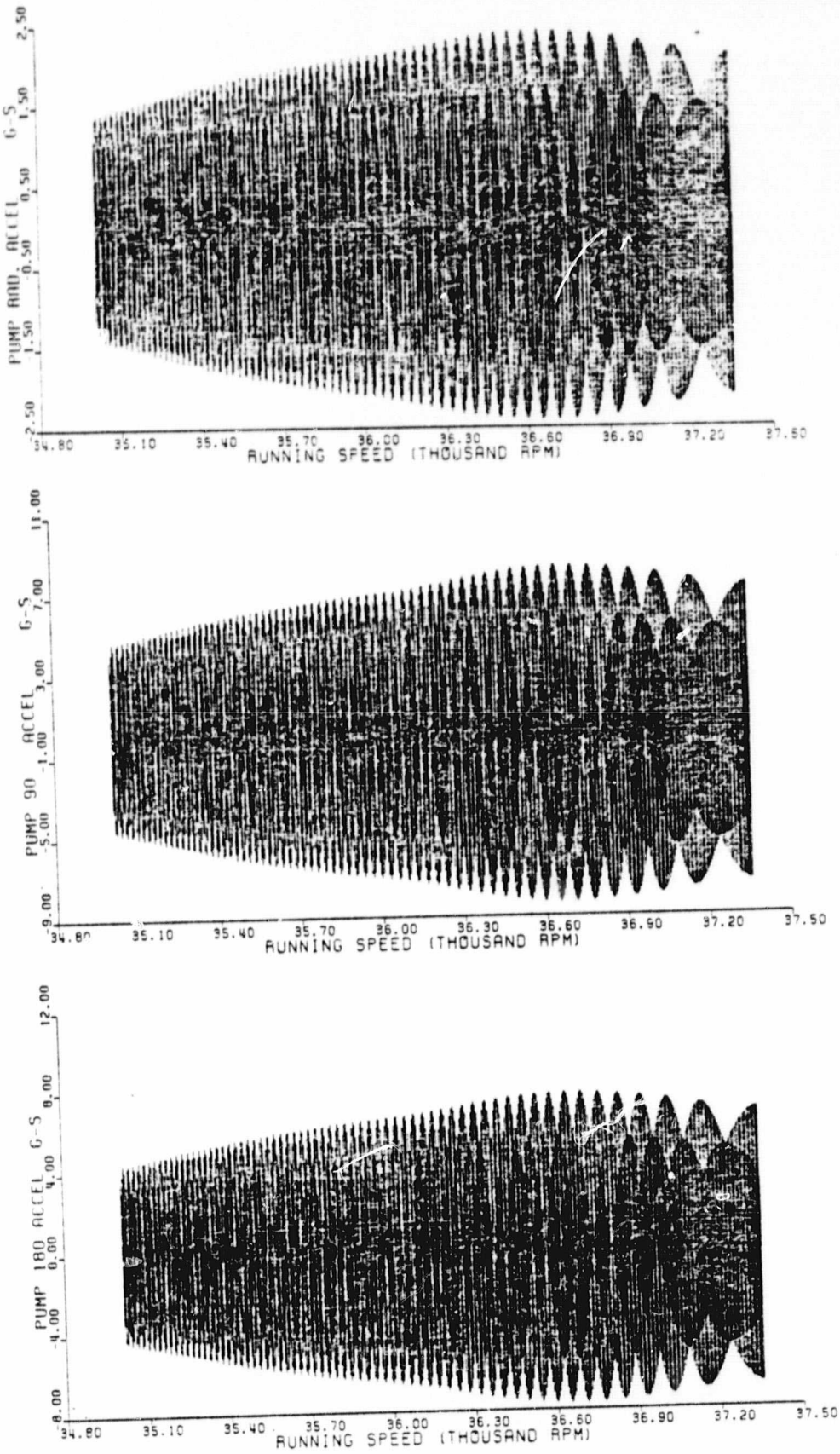

Figure 12 : Simulation of deceleration from FPL to RPL for the straight-seal configuration.

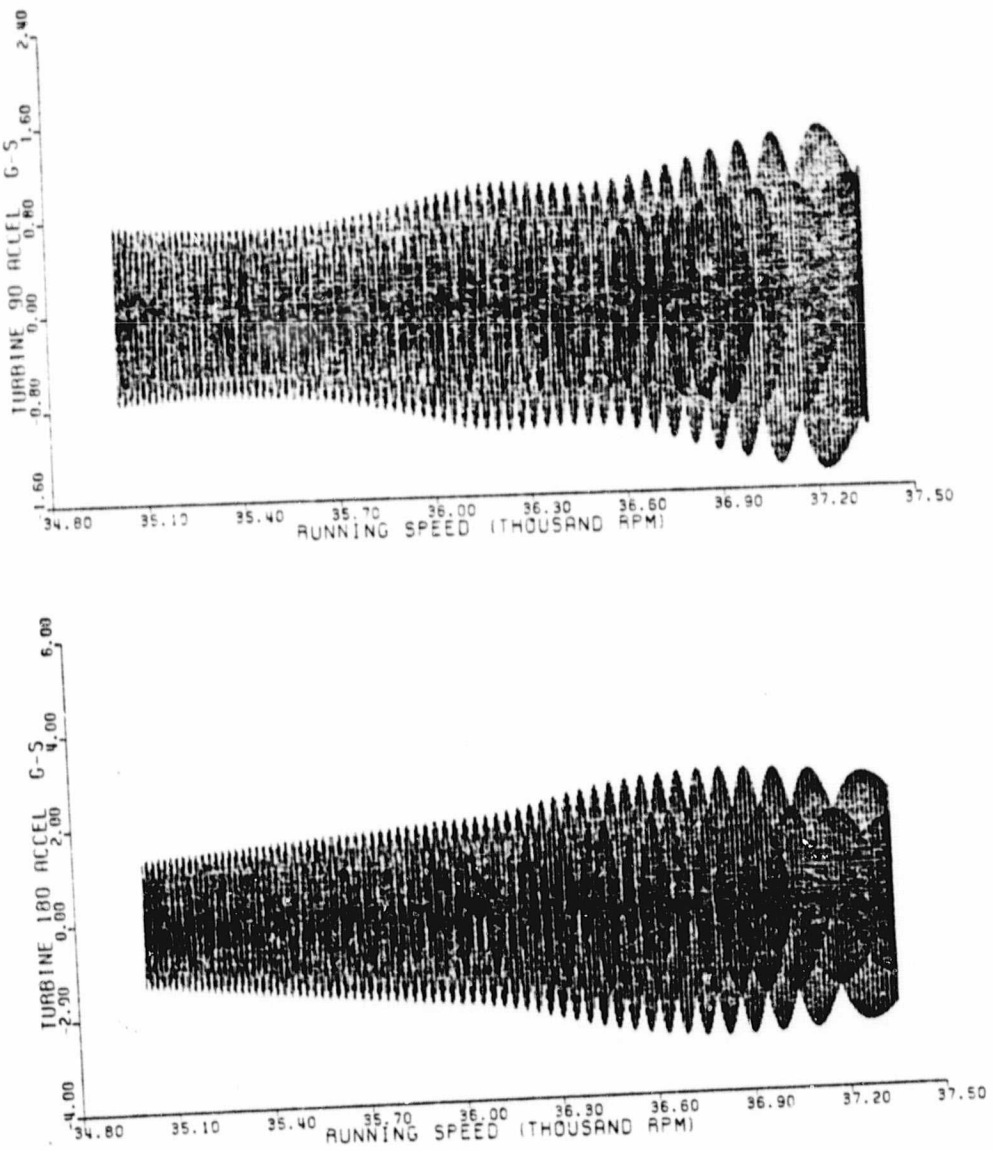

Figure 12 : Simulation of deceleration from FPL to RPL for the straight-seal configuration.

REFERENCES

1. Childs, D.W., "SSME Turbopump Technology Improvements via Transient Rotordynamic Analysis,: Final Report NASA Contract NAS8-31233, Mechanical Engineering Department, The University of Louisville, December 1975.

2. Childs, D.W., "The Space Shuttle Main Engine High-Pressure Fuel Turbopump Rotordynamic Instability Problem," ASME Trans., J. of Engin for Power, pp. 48-57, Jan. 1978.

3. Childs, D.W., "SSME Turbopump Technology Improvements via Transient Rotordynamic Analysis, Interim Progress Report," Mechanical Engineering Department, The University of Louisville, 25 July 1977.

4. Childs, D.W., Letter to Stephen Winder, ED 14, NASA-MSFC, 16 January 1980.

5. Childs, D.W., "Dynamic Analysis of Turbulent Annular Seals Based on Hirs' Lurication Equations," submitted to ASME Trans., J. of Lubrication Technology, Jan. 1980.

6. Alford, J.S., "Protecting Turbomachinery from Self-Excited Rotor Whirl," ASME Trans. J. of Engin. for Power, Series A. pp. 333-344, Oct. 1965.

7. Colding-Jorgensen, J., "The Effect of Fluid Forces on Rotor Stability of Centrifugal Compressors and Pumps," Workshop on Rotordynamic Instability Problems in High-Performance Turbomachinery, Texas A&M University 12-14 May 1980.

8. Childs, D.W., "Rotordynamics Analysis for the HPOTP (High Pressure Oxygen Turbopump) of the SSME (Space Shuttle Main Engine)," an interim progress report for NASA Contract NAS8-31233, The University of Louisville, Louisville, KY, 15 September 1979.

9. Yamamoto, T., "On the Critical Speeds of a Shaft," Memoirs of the Faculty of Engineering, Nagoya University, Vol. 6, No. 2, 1964.

APPENDIX A

INPUT DATA FOR THE HPFTP ROTORDYNAMICS MODEL

The fixed data used to define the rotordynamics model are provided in this appendix. Inch-lb-sec units are used throughout.

Rotor Eigenvalues

The rotor eigenvalues and eigenvectors used here are based on a structural-dynamic model by B. Rowan. The free-free eigenvalues used are listed below:

$\lambda_1 = 0$ $\qquad$ $\lambda_5 = 2048.6$ Hz

$\lambda_2 = 0$ $\qquad$ $\lambda_6 = 2622.7$ Hz

$\lambda_3 = 632.72$ Hz $\qquad$ $\lambda_7 = 3155.4$ Hz

$\lambda_4 = 1397.2$ Hz $\qquad$ $\lambda_8 = 3784.7$ Hz

Case Eigenvalues and Damping Factors

The case eigenvalues and eigenvectors are based on the most recent MSFC structural dynamic model. The eigenvalues used in this study are:

$\lambda_{c1} = 271.04$ Hz $\qquad$ $\lambda_{c6} = 561.79$ Hz

$\lambda_{c2} = 370.11$ Hz $\qquad$ $\lambda_{c7} = 564.99$ Hz

$\lambda_{c3} = 440.28$ Hz $\qquad$ $\lambda_{c8} = 609.84$ Hz

$\lambda_{c4} = 500.54$ Hz $\qquad$ $\lambda_{c9} = 706.10$ Hz

$\lambda_{c5} = 512.59$ Hz $\qquad$ $\lambda_{c10} = 730.64$ Hz

One-half percent of critical damping was used for all modes. These are the same modes used in the MSFC transient model.

Seal Dynamic Coefficients

The only seals of importance to the rotordynamic response of the HPFTP are the interstage seals. The coefficients for these seals are provided in Table 2(a) and Table 2(b).

	FPL	RPL	MPL
K	5.003×10^5	4.3981×10^5	2.4242×10^5
k	0.8187×10^5	0.7986×10^5	0.3275×10^5
C	102.3	94.2	64.8
c	13.34	13.10	7.562
M	6.242×10^{-3}	6.033×10^{-3}	5.144×10^{-3}

Table 2(a). Dynamic seal coefficients for straight smooth seals.

	FPL	RPL	MPL
K	1.247×10^5	1.098×10^5	0.6044×10^5
k	1.377×10^4	1.191×10^4	0.5458×10^4
C	20.49	18.91	12.99
c	1.317	1.194	0.688
M	5.374×10^{-4}	5.197×10^{-4}	4.939×10^{-4}

Table 2(b). Dynamic seal coefficients for smooth stepped seals.

Balance-Piston Stiffness and Dynamic Coefficients

The balance piston stiffness and damping coefficients are:

$$KZ = 2.6 \times 10^6 \quad , \quad CZ = 450.1$$

Bearing & Bearing Carrier Stiffness

The same bearing stiffness is used for all bearings, and is interpolated from the following data:

Speed	Zero	MPL	RPL	FPL
K_b	1.38×10^6	0.705×10^6	0.654×10^6	0.648×10^6

The bearing support stiffness used is:

$$K_s = 2.65 \times 10^6 \text{ lb/in.}$$

DYNAMIC ANALYSIS OF TURBULENT ANNULAR SEALS BASED ON HIRS' LUBRICATION EQUATION*

D. W. Childs
Mechanical Engineering Department
Speed Scientific School
The University of Louisville
Louisville, KY 40208

Expressions are derived which define dynamic coefficients for high-pressure annular seals typical of neck-ring and interstage seals employed in multi-stage centrifugal pumps. Completely developed turbulent flow is assumed in both the circumferential and axial directions, and is modeled in this analysis by Hirs' turbulent lubrication equations. Linear zeroth and first-order "short-bearing" perturbation solutions are developed by an expansion in the eccentricity ratio. The influence of inlet swirl is accounted for in the development of the circumferential flow field. Comparisons are made between the stiffness, damping, and inertia coefficients derived herein based on Hirs' model and previously published results based on other models. Finally, numerical results are presented for interstage seals in the Space Shuttle Main Engine High Pressure Fuel Turbopump.

---

*This work was supported in part by NASA Grant NAS8-31233 from the George C. Marshall Space Flight Center and NASA Grant NSG 3200 Lewis Research Center.

Nomenclature

a	Dimensionless coefficient defined in Eq. (11)
b	Dimensionless coefficient defined in Eq. (7)
B	Dimensionless coefficient defined by Eq. (20)
$\tilde{C},\tilde{c}$	Dimensionless seal damping coefficients defined by Eq. (28)
C	Nominal seal radial clearance (L)
E	Dimensionless coefficient defined by Eq. (29)
h	Seal radial clearance (L)
h_1	First order perturbation in h (L)
$\tilde{K},\tilde{k}$	Dimensionless seal stiffness coefficients defined by Eq. (28)
L	Seal length (L)
$m_0 = 0.066,\ n_0 = -0.25$	Coefficients for Hirs' turbulence equations
p	Fluid pressure (F/L^2)
p_i	Supply pressure at entrance (F/L^2)
p_0, p_1	Zeroth and first-order pressure perturbation (F/L^2)
$\Delta P = (1+\xi+2\sigma)\rho V^2/2$	Nominal pressure drop across seal (F/L^2)
R	Seal radius (L)
$R_C = \rho(R\omega)h/\mu$	Circumferential local Reynolds number
$R_a = \rho V h/\mu$	Axial local Reynolds number
$R_{C0} = \rho(R\omega)C/\mu$	Nominal circumferential Reynolds number
$R_{a0} = \rho VC/\mu$	Nominal axial Reynolds number
$U = R\omega$	(L/T)
u_z, u_θ	Axial and tangential fluid velocity components (L/T)
$U_z = u_z/R\omega,\ U_\theta = u_\theta/R\omega$	Dimensionless velocity components

$U_{z0}, U_{\theta 0}$	Zeroth order perturbations in U_z, U_θ
$U_{z1}, U_{\theta 1}$	First order perturbations in U_z, U_θ
v	Dimensionless inlet swirl defined as the solution to Eq. (10)
v_0	Initial (Z=0) swirl
V	Nominal axial velocity (L/T)
$z, R\theta$	Seal coordinates illustrated in figure 2 (L)
$Z = z/L$	Dimensionless axial seal position
X, Y	Radial seal displacements (L)
β	Dimensionless coefficient defined by Eq. (11)
ε	Eccentricity ratio introduced in Eq. (1)
ξ	Inlet pressure-loss coefficient
ρ	Fluid density (ML^{-2})
λ	Friction loss coefficient defined in Eq. (11)
$\sigma = \lambda L/C$	
$\tau = t/T$	Dimensionless time
ω	Shaft angular velocity (T^{-1})

Introduction

In a series of publications, Black and Jenssen [1,2,3,4] have explained the influence of seal forces on the rotordynamic behavior of pumps. Figure 1 illustrates the two seal types which have the potential for developing significant rotor forces. The neck or wear-ring seals are provided to reduce the back leakage flow along the front surface of the impeller face, while the interstage seal reduces the leakage from an impeller inlet back along the shaft to the back side of the preceding impeller. Black and Jenssen's work dealt primarily with boiler-feed pumps handling water. However, seals may have a significant influence on rotordynamic behavior of any multi-stage pump, e.g., reference [5] discusses the crucial dependence of the dynamic response of a hydrogen turbopump on its interstage seal design.

Black and Jenssen are responsible for the initial analytical development of dynamic stiffness and damping coefficients for high-pressure annular seals. Their coefficients are valid for small motion of the seal journal about a centered position relative to its bearing. A bulk-flow analysis is employed, with the circumferential bulk-flow velocity assumed to be fully developed shear flow at $\frac{R\omega}{2}$. The axial-flow momentum equation agrees with Yamada's [6] friction-loss results for rotating concentric cylinders, which defines the axial friction factor as a function of the axial and radial Reynolds numbers. In [4], Black and Jenssen define the friction factor as a function of the local axial and radial Reynolds numbers.

While Black and Jenssen's results apply only for small seal motion about a centered position, Allaire et al. [7] use Black's

model to numerically calculate dynamic coefficients at large eccentricities. Further, while Black and Jenssen define seal coefficients in a half-speed rotating reference system, and employ a coordinate transformation to achieve stationary-reference results, Allaire et al. perform all calculations in a stationary reference frame.

In an as yet unpublished result [8], Black has combined his prior seal-analysis governing equations with equations previously derived [9] for the analysis of, "Journal-bearings with high axial-flow in the turbulent regime," to examine the development of circumferential flow in a centered seal as a function of axial seal position. His results demonstrate that the bulk circumferential velocity of a fluid element asymptotically approaches $\frac{R\omega}{2}$ as it proceeds axially along the seal. The rate at which it approaches this limiting velocity depends on the amplitude of the axial and radial Reynolds numbers. Predictions of the stiffness cross-coupling term are generally reduced if the development of circumferential flow is accounted for in the analysis for stiffness and damping.

One of the problems involved in using and/or understanding Black and Jenssen's results is that various ad hoc governing equations are developed and used to obtain separate results. Further, the governing equations do not generally reduce to recognizable turbulent lubrication equations. Allaire and Lin [10] have partially remedied this deficiency by performing a numerical analysis for short seals based on Hirs'[11],[12] turbulent lubrication theory. However, they have retained Black's initial assumption of a one half speed circumferential velocity.

The present analysis also begins with Hirs' governing equation, but has the objective of developing analytical expressions for the seal dynamic coefficients incorporating all of Black and Jenssen's various developments. The development is based on a perturbation analysis of Hirs' equations in the eccentricity ratio ε, and yields results for a centered zero-eccentricity position.

Governing Equations

Figure 2 illustrates the seal geometry. Hirs' governing equations are provided in Appendix A and are thoroughly discussed in references [11] and [12]. We propose to expand these equations in terms of the perturbation variables

$$\begin{aligned} U_z &= U_{z0} + \varepsilon U_{z1} \quad , \quad h = C + \varepsilon h_1 \\ U_\theta &= U_{\theta 0} + \varepsilon U_{\theta 1} \quad , \quad p = p_0 + \varepsilon p_1 \end{aligned} \tag{1}$$

to obtain a "short bearing" solution. The short-bearing aspect of the solution is obtained by setting $\frac{\partial p}{\partial \theta} = 0$ in Eq. (A.2). Substitution of the above variables into the governing equations (A.1) through (A.3) yields the following zeroth-order axial

$$\frac{-C^2}{\mu U}\frac{\partial p_0}{\partial z} = \frac{n_0}{2} R_{C0}^{1+m_0}\{U_{z0}(U_{\theta 0}^2 + U_{z0}^2)^{\frac{1+m_0}{2}} + U_{z0}[(U_{\theta 0} - 1)^2 + U_{z0}^2]^{\frac{1+m_0}{2}}\} \tag{2}$$

and circumferential momentum equations

$$CU_{z0}\frac{\partial U_{\theta 0}}{\partial z} + \frac{n_0}{2} R_{C0}^{m_0}\{U_{\theta 0}(U_{\theta 0}^2 + U_{z0}^2)^{\frac{1+m_0}{2}} + (U_{\theta 0} - 1)[(U_{\theta 0} - 1)^2 + U_{z0}^2)]^{\frac{1+m_0}{2}}\} = 0 \tag{3}$$

The zeroth-order continuity equation is trivially satisfied.

The corresponding first-order axial momentum equation is

$$\frac{-C^2}{\mu U}\frac{\partial p_1}{\partial z} = \frac{2Ch_1}{\mu U}\frac{\partial p_0}{\partial z} + \frac{n_0}{2}(1+m_0)R_{C0}^{1+m_0}\left(\frac{h_1}{C}\right)U_{z0}\{(U_{\theta 0}^2 + U_{z0}^2)^{\frac{1+m_0}{2}} + [(U_{\theta 0} - 1)^2 + U_{z0}^2]^{\frac{1+m_0}{2}}\}$$

$$+ \frac{n_0}{2} R_{C0}^{1+m_0} U_{z1}\{(U_{\theta 0}^2 + U_{z0}^2)^{\frac{1+m_0}{2}} + [(U_{\theta 0} - 1)^2 + U_{z0}^2]^{\frac{1+m_0}{2}}\}$$

$$+ \frac{n_0}{2} R_{C0}^{1+m_0} U_{z0}(1+m_0)\{(U_{\theta 0}^2 + U_{z0}^2)^{\frac{m_0-1}{2}}(U_{\theta 0}U_{\theta 1} + U_{z0}U_{z1})$$

$$+ [(U_{\theta 0} - 1)^2 + U_{z0}^2]^{\frac{m_0-1}{2}}(U_{\theta 0}U_{\theta 1} + U_{z0}U_{z1} - U_{\theta 1})\}$$

$$+ R_{C0}\{\frac{C}{U}\frac{\partial U_{z1}}{\partial t} + U_{\theta 0}(\frac{C}{R})\frac{\partial U_{\theta 1}}{\partial \theta} + CU_{z0}\frac{\partial U_{z1}}{\partial z}\}\ , \qquad (4)$$

while the first-order circumferential-momentum equation is

$$0 = \frac{n_0}{2} R_{C0}^{m_0} U_{\theta 1}\{(U_{\theta 0}^2 + U_{z0}^2)^{\frac{1+m_0}{2}} + [(U_{\theta 0} - 1)^2 + U_{z0}^2]^{\frac{1+m_0}{2}}$$

$$+ \frac{n_0}{2} m_0 R_{C0}^{m_0}(\frac{h_1}{C})\{U_{\theta 0}(U_{\theta 0}^2 + U_{z0}^2)^{\frac{1+m_0}{2}}$$

$$+ (U_{\theta 0} - 1)[(U_{\theta 0} - 1)^2 + U_{z0}^2]^{\frac{1+m_0}{2}}\}$$

$$+ \frac{n_0}{2} R_{C0}^{m_0}(1+m_0)\{U_{\theta 0}(U_{\theta 0}^2 + U_{z0}^2)^{\frac{m_0-1}{2}}(U_{\theta 0}U_{\theta 1} + U_{z0}U_{z1})$$

$$+ (U_{\theta 0} - 1)[(U_{\theta 0} - 1)^2 + U_{z0}^2]^{\frac{m_0-1}{2}}(U_{\theta 0}U_{\theta 1} + U_{z0}U_{z1} - U_{\theta 1})\}$$

$$+ \frac{C}{U}\frac{\partial U_{\theta 1}}{\partial t} + U_{\theta 0}(\frac{C}{R})\frac{\partial U_{\theta 1}}{\partial \theta} + CU_{z0}\frac{\partial U_{\theta 1}}{\partial z} + h_1 U_{z0}\frac{\partial U_{\theta 0}}{\partial z} + CU_{y1}\frac{\partial U_{\theta 0}}{\partial z}\ , \qquad (5)$$

and the first-order continuity equation is

$$C\frac{\partial U_{z1}}{\partial z} + \frac{U_{\theta 0}}{R}\frac{\partial h_1}{\partial \theta} + \frac{h_1}{R}\frac{\partial U_{\theta 0}}{\partial \theta} + \frac{C}{R}\frac{\partial U_{\theta 1}}{\partial \theta} + \frac{1}{U}\frac{\partial h_1}{\partial t} = 0 \qquad (6)$$

Zeroth-Order Perturbation Solutions

We begin the solution of the equations by introducing the variables

$$U_{\theta 0} = \frac{1}{2} + v\ , \quad Z = z/L\ , \quad U_{z0} = \frac{V}{R\omega} = \frac{R_{a0}}{R_{C0}} = b \qquad (7)$$

into the zeroth-order circumferential momentum Eq. (3) to obtain

$$\frac{dv}{dZ} + B_1\left[\left(v + \frac{1}{2}\right)\left(\frac{1}{4} + v + v^2 + b^2\right)^{\frac{1+m_0}{2}} + \left(v - \frac{1}{2}\right)\left(\frac{1}{4} - v + v^2 + b^2\right)^{\frac{1+m_0}{2}}\right] = 0 \tag{8}$$

$$B_1 = \frac{n_o}{2b}\left(\frac{L}{C}\right) R_{C0}^{\ m_o} \tag{9}$$

The variable v defines the "swirl" of the circumferential flow in the sense that $v(Z) = 0$ implies that shear flow is uniformly established throughout the seal, i.e., $u_{\theta 0}(Z) = UU_{\theta 0} = \frac{R\omega}{2}$. Eq. (8) defines the development of circumferential velocity as a fluid element proceeds axially along the seal. It has the steady-state solution $v = 0$.

For small v, the linearized version of Eq. (8) is

$$\frac{dv}{dZ} + av = 0 \tag{10}$$

where

$$a = \sigma[1 + \beta(1+m_0)], \quad \beta = \frac{1}{1+4b^2} = \left(\frac{R\omega}{2V}\right)^2 / \left[1 + \left(\frac{R\omega}{2V}\right)^2\right]$$

$$\sigma = \frac{\lambda L}{C}, \quad \lambda = n_0 R_{a0}^{\ m_0}\left[1 + \frac{1}{4b^2}\right]^{\frac{1+m_0}{2}} \tag{11}$$

By comparison, Black [8] obtains the following definition

$$a = \sigma\left[1 + \beta^*\left(\frac{1+m_0}{2}\right)\right], \quad \beta^* = \frac{1}{1+\left(\frac{16}{7}b\right)^2}, \quad m_0 = -0.25 \tag{12}$$

The parameters β and β^* are different because Black retains Yamada's 1/7 power law velocity distribution, while Hirs does not.

However, the two parameters coincide at b = 0 and ∞, and are not markedly different over the complete range of b. The factor of two difference between $\beta(1+m_0)$ and $\beta^*(\frac{1+m_0}{2})$ follows from differences between Hirs' and Black's governing equations.

As things turn out, the solution to the linearized Eq. (10)

$$v = v_0 e^{-aZ} \tag{13}$$

is a very good approximation to the decidedly nonlinear Eq. (9), particularly for small magnitudes of v_0, the initial swirl. Figure 3 illustrates the maximum percentage error in v for $v_0 = -0.5$ and L/C = 100 (L/D = 1/2, C/R = 0.01) as a function of b for $R_{a0} = 3000$ and $R_{a0} = 200{,}000$. The worst error occurs at Z = 1 and was determined by numerically integrating Eq. (9), and comparing the result to the approximate solution of Eq. (13). The percentage error drops sharply as v_0 is moved from -0.5 towards zero. Figures 4 illustrates both a and e^{-a} as a function of b for $R_{a0} = 3000$ and $R_{a0} = 200{,}000$, and demonstrate that initial swirl will generally persist throughout the seal length. These results confirm Black's finding [8] that the 1/2 angular velocity assumption for circumferential flow throughout the seal is questionable in high axial flow seals if the inlet circumferential velocity differs substantially from the assumed 1/2 speed condition. In practical terms, neck-ring seals on pump impellers would normally have an imposed inlet circumferential velocity close to Rω/2, while interstage seals that are downstream of diffusers would have near-zero inlet circumferential velocities.

Returning to the zeroth-order axial momentum Eq. (2), and substituting from Eq. (7) for $U_{\theta 0}$ yields

$$\frac{\partial p_0}{\partial Z} = -\rho\sigma\, V^2\{1 + v^2\beta(m_0+1)[1 + 2\beta(m_0 - 1)] + \ldots \qquad (14)$$

Eq. (14) defines the nominal pressure gradient between two concentric rotating cylinders and should be comparable to Yamada's experimental result. In fact, Hirs [11] makes a comparison to Yamada's experimental results assuming $U_{\theta 0} = 1/2$ ($v_0 = 0$). Hirs' parameters are $n_0 = .066$, $m_0 = -0.25$ as compared to Yamada's values of $n_0 = .065$, $m_0 = -0.24$. Analysis of Yamada's experimental apparatus and results indicate that the v^2 terms in Eq. (13) would yield a decrease in calculated values of λ_0 of approximately 2% at $R_{a0} = 10{,}000$; $R_{C0} = 20{,}000$. For this Reynolds number set, Hirs' definition for λ_0* is approximately 20% too high. Hence, including v makes a small, but largely insignificant improvement in the correlation. Given that λ_0 is strongly dependent on R_{a0} and relatively independent of R_{C0}, these results are not surprising.

First-Order Perturbation Solutions

In the preceding analysis of the zeroth-order perturbation equations, terms of order v^2 and higher were shown to be negligible. If terms of this order are also neglected in the first-order axial-momentum Eq. (4), the result may be stated

$$\frac{\partial p_1}{\partial Z}/(\rho\sigma\, V^2) = (1-m_0)\left(\frac{h_1}{c}\right) - \frac{1}{b}[1 + \beta b^2(1+m_0)]U_{z1}$$
$$- \beta(1+m_0)\left[1 - \frac{\beta(1-m_0)}{4}\right]v_0 e^{-aZ}\, U_{\theta 1} \qquad (15)$$
$$- \frac{1}{\sigma b}\left[\frac{\partial U_{z1}}{\partial \tau} + \omega T\left(\frac{1}{2} + v_0 e^{-aZ}\right)\frac{\partial U_{z1}}{\partial \theta} + \frac{\partial U_{z1}}{\partial Z}\right]$$

where

$$\tau = \frac{t}{T} \quad , \quad T = \frac{L}{v} \quad , \quad \omega T = \frac{1}{b}\left(\frac{L}{R}\right)$$

Similarly, the circumferential-momentum Eq. (5) reduces to

$$0 = aU_{\theta 1} - a(1-m_0)\left(\frac{h_1}{C}\right)v_0 e^{-aZ} - \frac{a}{b}(1 - 4b^2A)v_0 e^{-aZ}\, U_{z1} + \frac{\partial U_{\theta 1}}{\partial \tau} + \omega T \left(\frac{1}{2} + v_0 e^{-aZ}\right) \frac{\partial U_{\theta 1}}{\partial \theta} + \frac{\partial U_{\theta 1}}{\partial Z} \tag{16}$$

where

$$A = \beta(1+m_0)[1 - \beta(1-m_0)]/[1 + \beta(1+m_0)]$$

Finally, the continuity Eq. (6) is stated

$$0 = \frac{\partial U_{z1}}{\partial Z} + \left(\frac{L}{R}\right)\left(\frac{1}{2} + v_0 e^{-aZ}\right) \frac{\partial}{\partial \theta}\left(\frac{h_1}{C}\right) + \left(\frac{L}{R}\right) \frac{\partial U_{\theta 1}}{\partial \theta} + b\, \frac{\partial}{\partial \tau}\left(\frac{h_1}{C}\right) \tag{17}$$

The axial-momentum Eq. (15) is similar to those developed by Black and Jenssen [1-4,8]; however, the term U_{z1}/b which appears in the second product on the right-hand side is $2U_{z1}/b$ in the above references. This discrepancy follows directly from differences between the governing equations of Hirs and Black.

Preceding analyses for seal stiffness and damping coefficients [1-4,8,10] have generally* neglected the first-order perturbation in the circumferential momentum, which eliminates $U_{\theta 1}$ as a variable,

---

*Black and Jensen [3] complete an approximate numerical solution including a small perturbation about a $U_\theta = \frac{R\omega}{2}$ assumed circumferential velocity.

and permits integration of Eq. (17) for U_{z1}, which may then be substituted into Eq. (15) to define $\frac{\partial p_1}{\partial Z}$. Eq. (15) is then integrated to define p_1, which is in turn integrated to determine seal reaction forces and stiffness and damping coefficients. In the present circumstances, one would prefer to solve the linear variable-coefficient Eqs. (16) and (17) for both $U_{\theta 1}$ and U_{z1}, substitute them into Eq. (15), and proceed to solve for p_1, etc. Unfortunately, efforts to analytically accomplish this preferred course of action have as yet been unsuccessful. A numerical solution comparable to that employed by Black and Jenssen [3] or a finite-difference procedure is apparently required to account for $U_{\theta 1}$. In the analysis which follows, $U_{\theta 1}$ is dropped and Black's initial analysis procedure followed. The general good agreement between Black's experimental and theoretical results certainly support this approach.

With $U_{\theta 1}$ eliminated, Eq. (17) is integrated to obtain

$$U_{z1} = U_{z10} - \left(\frac{L}{R}\right)\left[\frac{Z}{2} + \frac{v_0}{a}(1 - e^{-aZ})\right]\frac{\partial}{\partial\theta}\left(\frac{h_1}{C}\right) - bZ\left(\frac{h_1'}{C}\right) \qquad (18)$$

where the prime denotes differentiation with respect to τ, and

$$U_{z10} = U_{z1}(0,\theta,\tau)$$

Hence

$$\frac{\partial U_{z1}}{\partial Z} = -\left(\frac{L}{R}\right)\left(\frac{1}{2} + v_0 e^{-aZ}\right)\frac{\partial}{\partial\theta}\left(\frac{h_1}{C}\right) - b\left(\frac{h_1'}{C}\right)$$

$$\frac{\partial U_{z1}}{\partial \theta} = \frac{\partial U_{z10}}{\partial \theta} - \left(\frac{L}{R}\right)\left[\frac{Z}{2} + \frac{V_0}{a}(1 - e^{-aZ})\right]\frac{\partial^2}{\partial \theta^2}\left(\frac{h_1}{C}\right) - bZ\,\frac{\partial}{\partial \theta}\left(\frac{h_1'}{C}\right)$$

$$\frac{\partial U_{z1}}{\partial \tau} = \frac{\partial U_{z10}}{\partial \tau} - \left(\frac{L}{R}\right)\left[\frac{Z}{2} + \frac{V_0}{2}(1 - e^{-aZ})\right]\frac{\partial}{\partial \theta}\left(\frac{h_1'}{C}\right) - bZ\left(\frac{h_1''}{C}\right)$$

Substituting these results into Eq. (15) yields

$$\begin{aligned}\frac{\partial p_1}{\partial Z}/\rho\sigma V^2 = {} & (1-m_0)\left(\frac{h_1}{C}\right) \\ & - \frac{B}{b}\left\{U_{z10} - \left(\frac{L}{R}\right)\left[\frac{Z}{2} + \frac{V_0}{a}(1 - e^{-aZ})\right]\frac{\partial}{\partial \theta}\left(\frac{h_1}{C}\right) - bZ\left(\frac{h_1'}{C}\right)\right\} \\ & + \frac{1}{\sigma}\left[\omega T\left(\frac{1}{2} + V_0 e^{-aZ}\right)\frac{\partial}{\partial \theta}\left(\frac{h_1}{C}\right) + \left(\frac{h_1'}{C}\right)\right] \qquad (19) \\ & - \frac{1}{b\sigma}\left\{\frac{\partial U_{z10}}{\partial \tau} - \left(\frac{L}{R}\right)\left[\frac{Z}{2} + \frac{V_0}{2}(1 - e^{-aZ})\right]\frac{\partial}{\partial \theta}\left(\frac{h_1'}{C}\right) - bZ\left(\frac{h_1''}{C}\right)\right\} \\ & - \frac{\omega T}{b\sigma}\left(\frac{1}{2} + V_0 e^{-aZ}\right)\left\{\frac{\partial U_{z10}}{\partial \theta} - \left(\frac{L}{R}\right)\left[\frac{Z}{2} + \frac{V_0}{a}(1 - e^{-aZ})\right]\frac{\partial^2}{\partial \theta^2}\left(\frac{h_1}{C}\right)\right. \\ & \qquad \left. - bZ\,\frac{\partial}{\partial \theta}\left(\frac{h_1'}{C}\right)\right\}\end{aligned}$$

where

$$B = 1 + b^2\beta(1+m_0) \qquad (20)$$

Integration of this equation yields

$$\begin{aligned}\frac{p_1(Z,\theta,\tau)}{\rho\sigma V^2} = {} & \frac{p_1(0,\theta,\tau)}{\rho\sigma V^2} + Z(W_1 - W_2) + Z^2 W_3 \\ & + \frac{V_0}{a}(\omega T)\left(\frac{1}{\sigma} - \frac{B}{a}\right)(1 - e^{-aZ})\,\frac{\partial}{\partial \theta}\left(\frac{h_1}{C}\right) \\ & + \frac{V_0}{a\sigma}(\omega T)\left(\frac{1}{a} - \frac{1}{2}\right)(1 - e^{-aZ})\,\frac{\partial}{\partial \theta}\left(\frac{h_1'}{C}\right)\end{aligned}$$

$$- \frac{V_0}{ab\sigma}(\omega T)(1 - e^{-aZ}) \frac{\partial U_{z10}}{\partial \theta}$$

$$- \frac{V_0}{a\sigma}(\omega T\, Ze^{-aZ} [\frac{\omega T}{2} \frac{\partial^2}{\partial \theta^2}(\frac{h_1}{C}) + \frac{\partial}{\partial \vartheta}(\frac{h_1'}{C})] \tag{21}$$

where

$$W_1 = (1-m_0)(\frac{h_1}{C}) + \frac{1}{\sigma}(\frac{h_1'}{C}) + \omega T [B \frac{V_0}{a} + \frac{1}{2\sigma}]\frac{\partial}{\partial \theta}(\frac{h_1}{C}) \tag{22}$$

$$+ \frac{V_0}{2\sigma}(\omega T)\frac{\partial}{\partial \theta}(\frac{h_1'}{C}) + \frac{V_0}{2a\sigma}(\omega T)^2 \frac{\partial^2}{\partial \theta^2}(\frac{h_1}{C})$$

$$W_2 = \frac{B}{b} U_{z10} + \frac{1}{b\sigma} U'_{z10} + \frac{\omega T}{2b\sigma} \frac{\partial U_{z10}}{\partial \theta}$$

$$W_3 = \frac{B}{4}(\omega T) \frac{\partial}{\partial \theta}(\frac{h_1}{C}) + \frac{B}{2}(\frac{h_1'}{C}) + \frac{\omega T}{2\sigma} \frac{\partial}{\partial \theta}(\frac{h_1'}{C})$$

$$+ \frac{1}{2\sigma}(\frac{h_1''}{C}) + \frac{(\omega T)^2}{8\sigma} \frac{\partial^2}{\partial \theta^2}(\frac{h_1}{C})$$

The boundary conditions to be satisfied by the pressure are

$$p_i - p(0,\theta,\tau) = \frac{\rho}{2} u_z^2(0,\theta,\tau)(1+\xi),\ p(L,\theta,\tau) = 0 \tag{23}$$

These equations yield the following perturbation-variable boundary conditions at the seal inlet and exit, respectively

$$\frac{p_1(0,\theta,\tau)}{\rho\sigma V^2} = \frac{-(1+\xi)U_{z10}}{b\sigma}\ ,\ p_1(L,\theta,\tau) = 0 \tag{24}$$

Substituting from the first of Eq. (24) into Eq. (21), and evaluating the resultant pressure definition at Z = 1 yields the following definition for U_{z10}

$$\frac{\omega T}{b\sigma}\left[\frac{v_0}{a}(1 - e^{-a}) + \frac{1}{2}\right]\frac{\partial U_{z10}}{\partial\theta} + \frac{1}{b\sigma}U'_{z10} + \left[B + \frac{(1+\xi)}{\sigma}\right]\frac{U_{z10}}{b} =$$

$$W_1 + W_3 + \frac{v_0}{a}(\omega T)\left(\frac{1}{\sigma} - \frac{B}{a}\right)(1 - e^{-a})\frac{\partial}{\partial\theta}\left(\frac{h_1}{C}\right)$$

$$+ \frac{v_0}{a\sigma}(\omega T)\left[\left(\frac{1}{a} - \frac{1}{2}\right) - \left(\frac{1}{a} + \frac{1}{2}\right)e^{-a}\right]\frac{\partial}{\partial\theta}\left(\frac{h'_1}{C}\right)$$

$$- \frac{v_0 e^{-a}}{2a\sigma}(\omega T)^2\frac{\partial^2}{\partial\theta^2}\left(\frac{h_1}{C}\right) \qquad (25)$$

Time is not explicitly present on the right-hand side of this equation; hence, the partial derivative $U'_{z10} = \frac{\partial}{\partial\tau}(U_{z10})$ may arbitrarily be set to zero, which leaves a first order linear equation of the form

$$C\frac{dU_{z10}}{d\theta} + D\,U_{z10} = G$$

with the solution

$$U_{z10} = -U_{z10}(\theta = 0)e^{\frac{-D\theta}{C}} + \frac{G}{D}$$

The requirement of continuity, $U_{z10}(\theta) = U_{z10}(\theta + 2\pi)$, implies $U_{z10}(\theta = 0) = 0$, and yields the final solution

$$U_{z10} = \alpha\{W_1 + W_3 + \frac{v_0}{a}(\omega T)\left(\frac{1}{\sigma} - \frac{B}{a}\right)(1 - e^{-a})\frac{\partial}{\partial\theta}\left(\frac{h_1}{C}\right) \qquad (26)$$

$$+ \frac{v_0}{a\sigma}(\omega T)\left[\left(\frac{1}{a} - \frac{1}{2}\right) - \left(\frac{1}{a} + \frac{1}{2}\right)e^{-a}\right]\frac{\partial}{\partial\theta}\left(\frac{h'_1}{C}\right)$$

$$- \frac{v_0 e^{-a}}{2a\sigma}(\omega T)^2\frac{\partial^2}{\partial\theta^2}\left(\frac{h_1}{C}\right)\}$$

where

$$\alpha = b\sigma/(1+\xi + B\sigma)$$

Substitution for U_{z10} and $p_1(0,\theta,\tau)$ into Eq. (21) completes the definition for $p_1(Z,\theta,\tau)$.

Seal Dynamic Coefficients

The components of the reaction forces acting on the seal journal are defined by the integrals

$$F_X = -RL \int_0^{2\pi} \int_0^1 p \cos\theta \, dZd\theta = -\varepsilon RL \int_0^{2\pi} \bar{p}_1 \cos\theta d\theta$$

$$F_Y = -RL \int_0^{2\pi} \int_0^1 p \sin\theta \, dZd\theta = -\varepsilon RL \int_0^{2\pi} \bar{p}_1 \sin\theta d\theta \qquad (27)$$

where

$$\bar{p}_1 = \int_0^1 p_1 dZ$$

is the force per unit circumference defined by

$$\frac{\sigma \bar{p}_1(\theta)}{\Delta P} = - \tilde{K}\left(\frac{h_1}{C}\right) - \tilde{k} \frac{\partial}{\partial\theta}\left(\frac{h_1}{C}\right) - \tilde{C}\left(\frac{h_1'}{C}\right) - \tilde{c} \frac{\partial}{\partial\theta}\left(\frac{h_1'}{C}\right) - \tilde{m}\left(\frac{h_1''}{C}\right)$$

Further,

$$\tilde{K} = \frac{2\sigma^2}{(1+\xi+2\sigma)}\left\{E(1-m_0) - \frac{(\omega T)^2}{4\sigma}\left\{\frac{1}{2}\left(\frac{1}{6} + E\right) + \frac{2v_0}{a}\left[\left(E+\frac{1}{a^2}\right)(1-e^{-a}) - \left(\frac{1}{2}+\frac{1}{a}\right)e^{-a}\right]\right\}\right\}$$

$$\tilde{k} = \frac{\sigma^2(\omega T)}{(1+\xi+2\sigma)}\left\{\frac{E}{\sigma} + \frac{B}{2}\left(\frac{1}{6} + E\right) + \frac{2v_0}{a}\left\{EB + \left(\frac{1}{\sigma} - \frac{B}{a}\right)\left[(1-e^{-a})\left(E+\frac{1}{2}+\frac{1}{a}\right)-1\right]\right\}\right\}$$

$$\tilde{C} = \frac{2\sigma^2}{1+\xi+2\sigma}\left[\frac{E}{\sigma} + \frac{B}{2}\left(\frac{1}{6} + E\right)\right] \quad , \quad \tilde{m} = \frac{\sigma\left(\frac{1}{6}+E\right)}{(1+\xi+2\sigma)} \tag{28}$$

$$\tilde{c} = \frac{2\sigma(\omega T)}{(1+\xi+2\sigma)}\left\{\frac{1}{2}\left(\frac{1}{6} + E\right) + \frac{V_0}{a}\left\{\frac{Ea}{2} + \left(\frac{1}{a}-\frac{1}{2}\right)\left(E+\frac{1}{a}-\frac{1}{2}\right) + \frac{1}{a^2}\right.\right.$$

$$\left.\left. - e^{-a}\left[\left(\frac{1}{2}+E\right)\left(\frac{1}{2}+\frac{1}{a}\right) + \frac{1}{2a}\left(1+\frac{4}{a}\right)\right]\right\}\right\}$$

and

$$E = (1+\xi)/2(1 + \xi + B\sigma) \tag{29}$$

The clearance h is defined in terms of the components of the seal journal displacement vector by

$$h = C - X\cos\theta - Y\sin\theta$$

Hence

$$\frac{\varepsilon h_1}{C} = -\left(\frac{X}{C}\right)\cos\theta - \left(\frac{Y}{C}\right)\sin\theta$$

$$\varepsilon\frac{\partial}{\partial\theta}\left(\frac{h_1}{C}\right) = \left(\frac{X}{C}\right)\sin\theta - \left(\frac{Y}{C}\right)\cos\theta \ ,$$

etc., for the remaining derivatives. Substituting for $\left(\frac{h_1}{C}\right)$ and its derivatives into Eq. (27) yields the following definitions for the force components

$$-\frac{\lambda}{\pi R\Delta P}\begin{Bmatrix} F_X \\ F_Y \end{Bmatrix} = \begin{bmatrix} \tilde{K} & \tilde{k} \\ -\tilde{k} & \tilde{K} \end{bmatrix}\begin{Bmatrix} X \\ Y \end{Bmatrix} + T\begin{bmatrix} \tilde{C} & \tilde{c} \\ -\tilde{c} & \tilde{C} \end{bmatrix}\begin{Bmatrix} \dot{X} \\ \dot{Y} \end{Bmatrix} + T^2\begin{bmatrix} \tilde{m} & 0 \\ 0 & \tilde{m} \end{bmatrix}\begin{Bmatrix} \ddot{X} \\ \ddot{Y} \end{Bmatrix} \tag{30}$$

If $v_0 = 0$, these equations may be stated in the following format comparable to Black and Jenssen [3]

$$-\frac{\lambda}{\pi R\Delta P}\begin{Bmatrix} F_X \\ F_Y \end{Bmatrix} = \begin{bmatrix} \mu_0 - \mu_2(\omega T)^2/4 & \mu_1(\omega T)/4 \\ -\mu_1(\omega T)/4 & \mu_0 - \mu_2(\omega T)^2/4 \end{bmatrix}\begin{Bmatrix} X \\ Y \end{Bmatrix} + T\begin{bmatrix} \mu_1 & \mu_2\omega T \\ -\mu_2\omega T & \mu_1 \end{bmatrix}\begin{Bmatrix} \dot{X} \\ \dot{Y} \end{Bmatrix}$$

$$+ T^2\begin{bmatrix} \mu_2 & 0 \\ 0 & \mu_2 \end{bmatrix}\begin{Bmatrix} \ddot{X} \\ \ddot{Y} \end{Bmatrix} \qquad (31)$$

where

$$\mu_0 = \frac{2\sigma^2 E(1-m_0)}{1+\xi+2\sigma}\ , \quad \mu_2 = \frac{\sigma(\frac{1}{6}+E)}{1+\xi+2\sigma}$$

$$\mu_1 = \frac{\sigma^2}{1+\xi+2\sigma}\left[\frac{E}{\sigma} + \frac{B}{2}(\frac{1}{6} + E)\right] \qquad (32)$$

Figures 5 illustrates both these functions and the comparable functions μ_0^*, μ_1^*, μ_2^* from Black and Jenssen [3]. The functions μ_0, μ_1 are quite comparable to μ_0^*, μ_1^*, but are less sensitive to changes in b. For b = 0, μ_0 and μ_0^* coincide and the differences between μ_1 and μ_1^* are minimum (with respect to b). Although the functions μ_2 and μ_2^* differ significantly in magnitude, particularly for small values of σ, these parameters generally have a minimal influence on rotordynamic response. The fact that μ_2 is larger than μ_2^* implies simply that a Hirs-based model predicts larger "added-mass" values than those predicted by Black and Jenssen.

Numerical Results

As noted earlier, experience [5] has demonstrated that interstage seal characteristics are crucial to the rotordynamic stability of the SSME (Space Shuttle Main Engine) HPFTP (High Pressure Fuel Turbopump). The present interstage seal configuration has three annular segments at different diameters separated by two steps. A proposed alternative configuration eliminates the steps to yield a single-segment seal with the following nominal dimensions

$$D = 7.98 \times 10^{-2}, \quad L = 0.432 \times 10^{-2}, \quad C = 1.397 \times 10^{-4}$$

The nominal operating points of the turbopump are FPL (Full Power Level), RPL (Rated Power Level) and MPL (Minimum Power Level) with the following speeds, density, viscosity, and ΔP conditions:

	ω(RPM)	ρ	μ	ΔP
FPL	37,360	70.28	1.160×10^{-5}	1.492×10^{7}
RPL	35,020	68.0	1.086×10^{-5}	1.314×10^{7}
MPL	23,720	58.0	0.759×10^{-5}	7.260×10^{6}

Table 1 contains the seal dynamic coefficients corresponding to these conditions for $v_0 = 0$ and $v_0 = -0.5$. Inlet swirl causes a sharp drop in the cross-coupled stiffness and damping coefficients k and c, and a slight increase in the direct stiffness coefficient K, with C and m unchanged. Stability predictions for the HPFTP would obviously be substantially improved if the coefficients of Table 1(a) are employed rather than those of Table 1(b), because of the markedly smaller values of cross-coupling coefficient k.

	MPL	RPL	FPL
K	0.5638×10^8	1.0229×10^8	1.636×10^8
k	0.7278×10^7	1.5751×10^7	1.820×10^7
C	14,390.	20,950.	22,730.
c	1,418.	2,457.	2,711.
m	0.9674	1.135	1.174

Table 1(a). HPFTP dynamic coefficients for $v_0 = -0.5$.

	MPL	RPL	FPL
K	0.54573×10^8	0.9769×10^8	1.1093×10^8
k	1.7875×10^7	3.8417×10^7	4.4455×10^7
C	14.390.	20,950.	22,730.
c	2,403.	4,161.	4,590.
m	0.9674	1.135	1.174

Table 1(b). HPFTP dynamic coefficients for $v_0 = 0$.

REFERENCES

1. H. F. Black, "Effects of Hydraulic Forces in Annular Pressure Seals on the Vibrations of Centrifugal Pump Rotors," J. M.Eng. Sci., Vol. 11, No. 2, pp. 206-213, 1969.

2. D. N. Jenssen, "Dynamics of Rotor Systems Embodying High Pressure Ring Seals," Ph.D. Dissertation, Heriot-Watt University, Edinburgh, Scotland, July 1970.

3. H. F. Black and D. N. Jenssen, "Dynamic Hybrid Properties of Annular Pressure Seals," Proc. J. Mech. Engin., Vol. 184, pp. 92-100, 1970.

4. H. F. Black and D. N. Jenssen, "Effects of High-Pressure Ring Seals on Pump Rotor Vibrations," ASME Paper No. 71-WA/FF-38, 1971.

5. D. W. Childs, "The Space Shuttle Main Engine High-Pressure Fuel Turbopump Rotordynamic Instability Problem," ASME Transactions, Engineering for Power, pp. 48-57, Jan. 1978.

6. Y. Yamada, "Resistance of Flow through an Annulus with an Inner Rotating Cylinder," Bull. J.S.M.E., Vol. 5, No. 18, pp. 302-310, 1962.

7. P. E. Allaire, E. J. Gunter, C. P. Lee, and L. E. Barrett, "The Dynamic Analysis of the Space Shuttle Main Engine High Pressure Fuel Turbopump Final Report, Part II, Load Capacity and Hybrid Coefficients for Turbulent Interstage Seals," University of Virginia Report UVA/528140/ME76/103, September 1976.

8. H. F. Black, "The Effect of Inlet Flow Swirl on the Dynamic Coefficients of High-Pressure Annular Clearance Seals," unpublished analyses performed at the University of Virginia, August 1977.

9. H. F. Black, "On Journal Bearings with High Axial Flows in the Turbulent Regime," J. of Mech. Eng. Sci., Vol. 12, No. 4, pp. 301-303, 1970.

10. P. E. Allaire and Y-J. Lin, "Linearized Dynamic Analysis of Plain Short Turbulent Seals," submitted to ASME J. of Lub. Technology.

11. G. G. Hirs, "Fundamentals of a Bulk-Flow Theory for Turbulent Lubrication Films " Ph.D. Dissertation, Delft Technical University, The Netherlands, July 1970.

12. G. G. Hirs, "A Bulk-Flow Theory for Turbulence in Lubricant Films," ASME J. of Lub. Tech., pp. 137-146, April 1973.

Appendix A: Hirs Turbulent Lubrication Equations

Hirs' turbulent lubrication equations [11],[12] is a bulk-flow theory which does not explicitly make any assumptions concerning either (a) local flow velocity due to turbulence, or (b) the shape of average flow-velocity profiles. Only the bulk-flow relative to a surface or wall and the corresponding shear stress at that surface or wall are considered or correlated. Hirs' axial and circumferential momentum equations can be stated, respectively, as

$$\frac{-h^2}{\mu U}\frac{\partial p}{\partial z} = \frac{n_0}{2} R_C^{1+m_0}\{U_z(U_\theta^2 + U_z^2)^{\frac{1+m_0}{2}} + U_z[(U_\theta - 1)^2 + U_z^2]^{\frac{1+m_0}{2}}\}$$
$$+ R_C\{\frac{h}{U}\frac{\partial U_z}{\partial t} + \frac{hU_\theta}{R}\frac{\partial U_z}{\partial \theta} + hU_z\frac{\partial U_z}{\partial z}\} \qquad (A.1)$$

$$\frac{-h^2}{\mu U}\frac{1}{R}\frac{\partial p}{\partial \theta} = \frac{n_0}{2} R_C^{1+m_0}\{U_\theta(U_\theta^2 + U_z^2)^{\frac{1+m_0}{2}} + (U_\theta - 1)[(U_\theta - 1)^2 + U_z^2]^{\frac{1+m_0}{2}}\}$$
$$+ R_C\{\frac{h}{U}\frac{\partial U_\theta}{\partial t} + \frac{hU_\theta}{R}\frac{\partial U_\theta}{\partial \theta} + hU_z\frac{\partial U}{\partial z}\} \qquad (A.2)$$

with the bulk-flow momentum equation

$$h\frac{\partial U_z}{\partial z} + \frac{1}{R}\frac{\partial}{\partial \theta}(hU_\theta) + \frac{1}{R\omega}\frac{\partial h}{\partial t} = 0 \qquad (A.3)$$

List of Figures

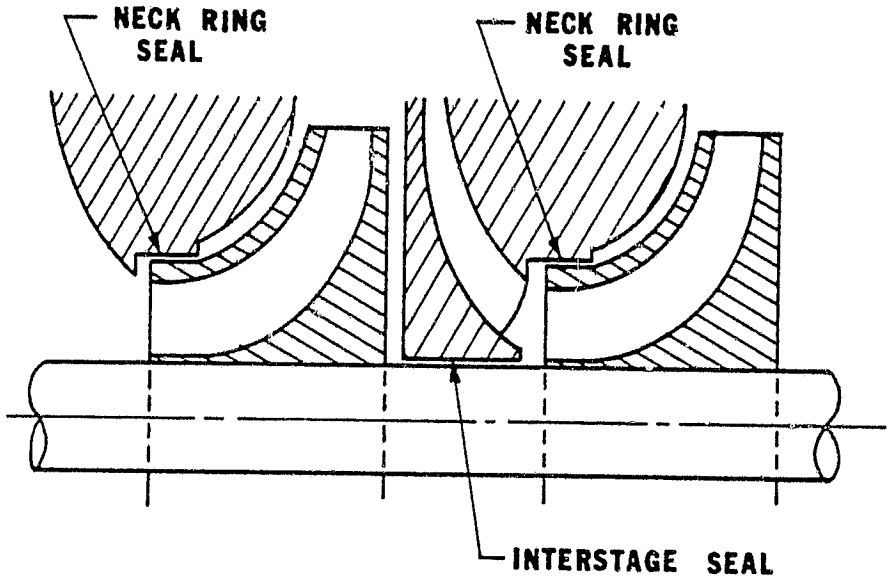

Fig. 1

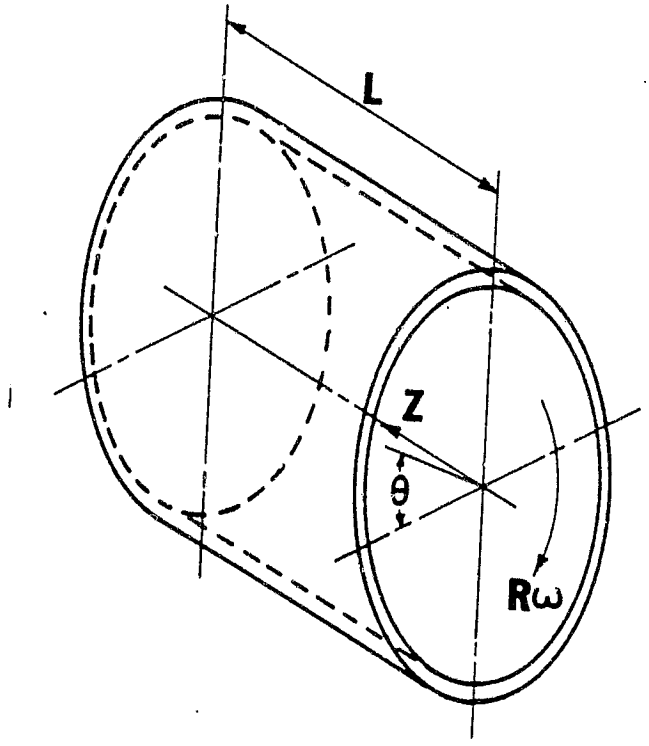

Fig. 2

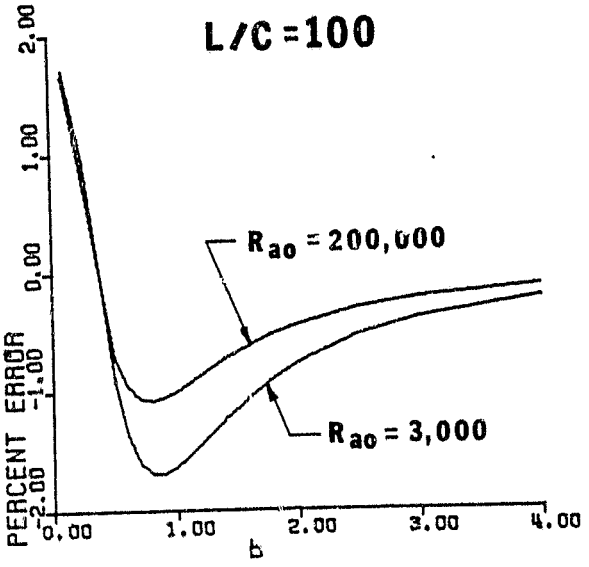
L/C =100
R_{ao} = 200,000
R_{ao} = 3,000
PERCENT ERROR
2.00
1.00
0.00
-1.00
-2.00
0.00
1.00
2.00
3.00
4.00
b

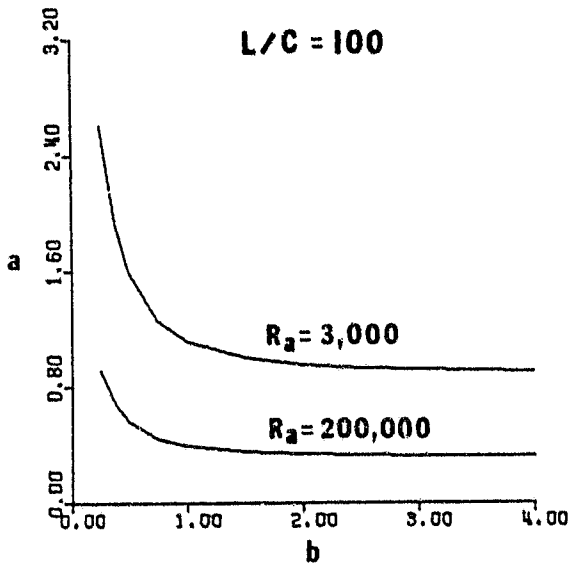
L/C = 100
a
3,20
2,40
1,60
0,80
0,00
R_a = 3,000
R_a = 200,000
0.00
1.00
2.00
3.00
4.00
b

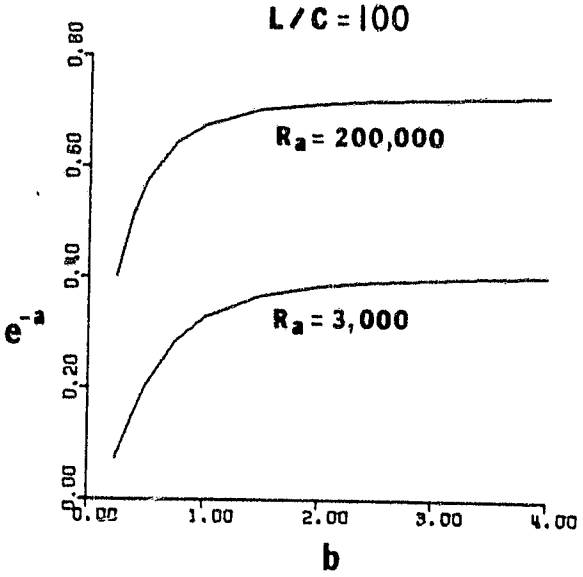
L/C = 100
e^{-a}
0,80
0,60
0,40
0,20
0,00
R_a = 200,000
R_a = 3,000
0.00
1.00
2.00
3.00
4.00
b

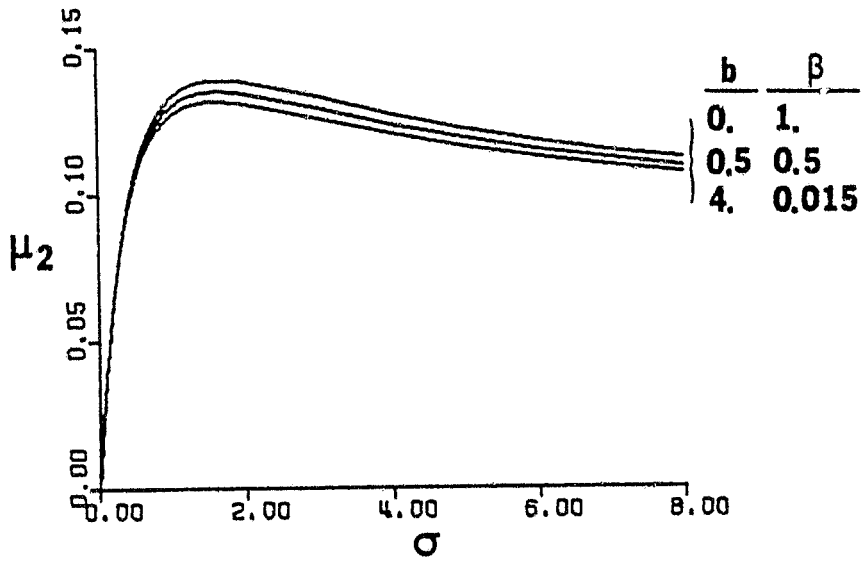
μ2
0,15
0,10
0,05
0,00
0.00
2.00
4.00
6.00
8.00
σ
b β
0. 1.
0.5 0.5
4. 0.015

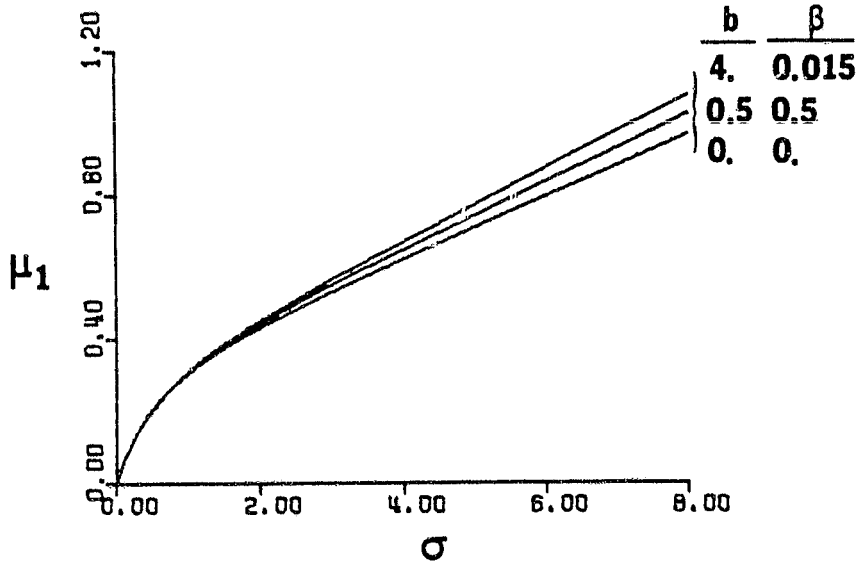
μ1
1,20
0,80
0,40
0,00
0.00
2.00
4.00
6.00
8.00
σ
b β
4. 0.015
0.5 0.5
0. 0.

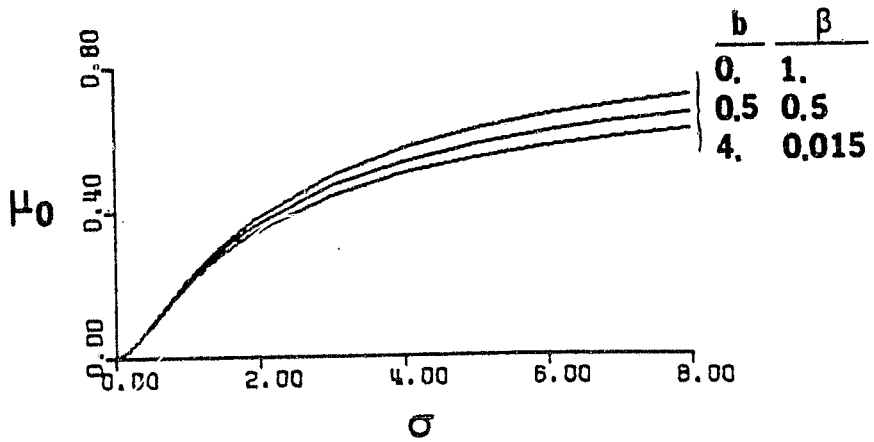
μ0
0,80
0,40
0,00
0.00
2.00
4.00
6.00
8.00
σ
b β
0. 1.
0.5 0.5
4. 0.015

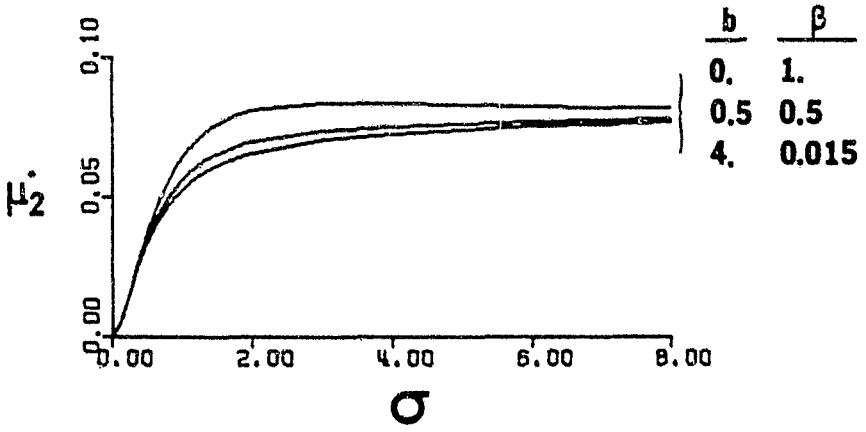
b β
0. 1.
0.5 0.5
4. 0.015
μ2
0.10
0.05
0.00
0.00
2.00
4.00
6.00
8.00
σ

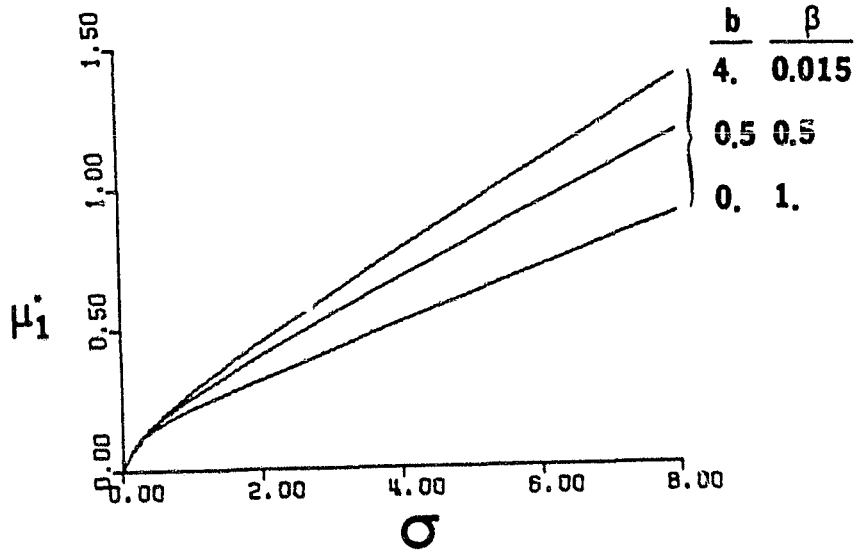
b β
4. 0.015
0.5 0.5
0. 1.
μ1
1.50
1.00
0.50
0.00
0.00
2.00
4.00
6.00
8.00
σ

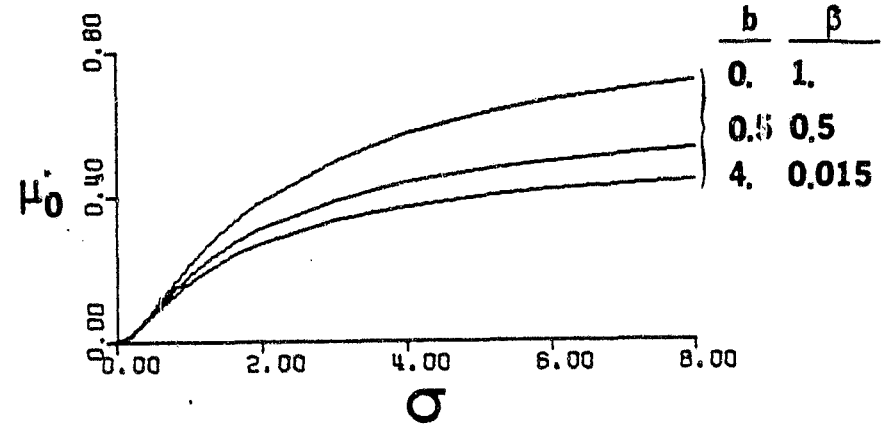
b β
0. 1.
0.5 0.5
4. 0.015
μ0
0.80
0.40
0.00
0.00
2.00
4.00
6.00
8.00
σ

NASA—MSFC—C